

## Assessing the ability of numerical ice sheet models to simulate grounding line migration

A. Vieli and A. J. Payne

Centre for Polar Observation and Modelling, School of Geographical Sciences, University of Bristol, Bristol, UK

Received 6 July 2004; revised 19 October 2004; accepted 12 November 2004; published 21 January 2005.

[1] Grounding line migration is a key process affecting the stability of marine ice sheets such as the West Antarctic ice sheet (WAIS). Grounding line motion is often included in numerical models simulating the past and future evolution of the WAIS; however, little attention has been paid to the numerical consistency of these models. The aim of this paper is to assess the ability of simple versions of existing marine ice sheet models to simulate grounding line migration. In particular, we investigate the response of the grounding line to external forcing and the sensitivity of the models' predictions to their numerics and the mechanical coupling between ice sheet and shelf. From the model comparison, there is no consensus on how the grounding line should react to changes in boundary conditions. A crucial finding is the strong dependency of models using a fixed grid on numerical details such as the horizontal grid size. This implies that we should be very wary about grounding line predictions from such models. Including mechanical coupling at the grounding line does not seem to change the qualitative behavior of the models. This suggests that the way the grounding line is treated in marine ice sheet models dominantly determines the grounding line dynamics. We find that models that employ a moving grid to explicitly track the grounding line do not share many of the deficiencies of the fixed grid models. We conclude that at present, no reliable model of the grounding line is available, and further model development is urgently needed.

**Citation:** Vieli, A., and A. J. Payne (2005), Assessing the ability of numerical ice sheet models to simulate grounding line migration, *J. Geophys. Res.*, 110, F01003, doi:10.1029/2004JF000202.

### 1. Introduction

[2] This paper aims to assess the ability of numerical ice sheet models to simulate the migration of the grounding line. In particular, we compare the grounding line dynamics predicted by a range of models of marine ice sheets, and investigate the influence of numerics on these predictions. We further investigate the role of mechanical coupling over the grounding line in determining the migration of the grounding line.

[3] Marine ice sheets rest on a bed well below sea level and drainage usually takes place through floating ice shelves. The stability of a marine ice sheet is thought to be controlled by the dynamics of the grounding line (the junction between the grounded ice sheet and a floating ice shelf or the ocean). Glaciologists generally agree that marine ice sheets are more likely to undergo rapid change than land-based ice sheets [Bentley, 1998].

[4] Most parts of the present-day West Antarctic ice sheet (WAIS) are well below sea level and this has led various authors to speculate on its stability. In the past, the WAIS has grown and shrunk and may even have disappeared entirely, however we do not know in detail how rapidly these changes occurred [Alley and Bindschadler, 2001].

There is however strong evidence that the marine portions of the Eurasian ice sheet disintegrated within a short time [Siebert and Dowdeswell, 2002]. Although changes in the WAIS are likely to be linked to changes in global sea level, there is little direct correlation in the timing of deglaciation and sea level rise [Anderson and Shipp, 2001; Conway *et al.*, 1999]. If the entire WAIS were discharged into the ocean, global sea level would rise by 5 to 6 m [Bentley, 1998]. The magnitude of this effect has led to the identification of the future of the WAIS as a key uncertainty in our ability to predict future sea level change. Accurate modeling of the migration of the grounding line is therefore crucial to the validity of these predictions.

[5] Up to the present, only a few attempts have been made to simulate grounding line migration within marine ice sheet models, and none of these simulations explicitly considers ice stream dynamics. Such models can be divided into two main classes. The first group of numerical models considers an ice sheet that is coupled mechanically and/or through the thickness evolution equation to an ice shelf and a flotation criterion is used to identify whether ice is grounded or floating at a particular grid point [Huybrechts, 1990; Ritz *et al.*, 2001; Van der Veen, 1985]. In general, these models use a fixed horizontal grid and have mainly been used to reconstruct the evolution of Antarctica [Huybrechts and De Wolde, 1999; Huybrechts, 2002; Ritz *et al.*, 2001]. They show a thinning and retreat during the most

recent deglaciation, which approximately follows the external sea level forcing and therefore contradicts the observation that postglacial retreat along the Siple Coast occurred very late [Anderson and Shipp, 2001; Conway *et al.*, 1999].

[6] Furthermore, these models incorporate a static ice stream hydrology (an effective pressure-dependent sliding relation with water pressure set to sea level) that is believed to be crucial in allowing the modeled WAIS to undergo substantial retreat but whose validity is somewhat suspect [see Hindmarsh and LeMeur, 2001]. This means that the retreat and thinning produced by these models may be occurring for the wrong reasons. In addition, the grounding line motion is found to be rather sensitive to the computed temperature (effective viscosity) within the ice shelves [Huybrechts and De Wolde, 1999]. More importantly, the grounding line motion predicted in these models has yet to be shown to be independent of the models' numerics.

[7] A second group of models only considers the grounded part of a marine ice sheet and does not include mechanical coupling or coupling through mass conservation at the grounding line. Several studies indicate that longitudinal coupling at the grounding line is less important than previously supposed [Hindmarsh, 1993; Whillans and Van der Veen, 1993; Echelmeyer *et al.*, 1994; Bentley, 1997]. A further argument for ignoring the ice shelf is that if the grounded part of a marine ice sheet is sufficiently described by the shallow ice approximation (SIA [Hutter, 1983]), in which the gravitational driving stresses are exclusively balanced by local vertical stress gradients, then longitudinal stresses are not significant and coupling with the shelf can not be important [Hindmarsh and LeMeur, 2001]. Hindmarsh [1996] has explicitly shown that a marine ice sheet, that is described by the SIA and which has no mechanical coupling to an ice shelf, exhibits neutral equilibria. This means the equilibrium position is continuous and that an infinity of equilibrium configurations exists [Hindmarsh, 1993]. Furthermore, he showed that for marine ice sheets the neutral equilibrium is an attractive state, meaning the system is stable and finds a steady state after a small perturbation. These models use a stretched horizontal grid and the motion of the grounding line is calculated using a prognostic equation. Their dynamics are shown to be consistent with their underlying differential equations (which imply neutral equilibrium). A detailed description of these models and their dynamics are given by Hindmarsh [1996], LeMeur and Hindmarsh [2001], and Hindmarsh and LeMeur [2001].

[8] One important result from these studies is that sea level changes alone can not explain the observed 500 km retreat of the WAIS during the most recent deglaciation [LeMeur and Hindmarsh, 2001]. However, the inclusion of internal oscillations, either specified or generated via the MacAyeal-Payne thermal mechanism, does produce the observed range of grounding line migration [Hindmarsh and LeMeur, 2001]. Whether one can generally ignore mechanical coupling and/or coupling through the mass conservation at the grounding line is still an open question. In particular, it seems likely that coupling between ice streams (where the SIA is not applicable) and shelves must be stronger than between sheets (obeying SIA) and shelves.

[9] Up to the present, the dynamics of the grounding line are poorly understood and no clear picture is available on

how the grounding line should react to a change in external forcing. This study therefore tries to compare the different ways of treating grounding line migration within marine ice sheet models. This includes the influence of numerical details and discretization on the dynamics of the grounding line, as well as the importance of mechanical coupling at the grounding line.

[10] This assessment is undertaken on "simple" versions of the two different model groups discussed above. The main simplifications are that only plane flow is considered and the ice sheet is assumed to be isothermal. Furthermore, isostatic adjustment of the bed is not considered. Although, these simplifications may limit quantitative model predictions, they do not affect the main aim of this study, which is to compare different grounding line migration models and to test whether these models depend on their numerics. If the behavior of these simplified one-dimensional plane flow models is dependent on their numerics (or the way in which the grounding line is treated), then the original large-scale two-dimensional models are also expected to show these dependencies. By deliberately choosing to work with simplified models, we hope to be able to identify these dependencies more easily than is the case with more complex models, where many processes are likely to affect grounding line motion and assessing cause and effect is consequently more difficult.

## 2. Model Descriptions

[11] This study focusses on the numerical modeling of the evolution of a marine ice sheet with or without an ice shelf, and in particular on modeling the migration of the grounding line. All the models used in this paper are two-dimensional isothermal plane flow models, that means the rate factor is constant throughout the ice sheet and only flow and thickness changes in  $x$  direction are considered and in  $y$  direction the ice body is assumed to extend infinitely. The  $z$  coordinate is the vertical direction and is positive upward.

### 2.1. Governing Equations

[12] The evolution of the ice thickness of a marine ice sheet for plane flow is described by

$$\frac{\partial h}{\partial t} = a - \frac{\partial q}{\partial x}, \quad (1)$$

where  $t$  is the time,  $a$  the accumulation rate and  $q$  is the horizontal flux of ice through a vertical column of ice with thickness  $h$  and is given by  $q = hu$ , where  $u$  is the vertically averaged horizontal ice velocity.

[13] In this study we consider the three distinct flow regimes of a marine ice sheet, namely ice sheets, ice streams and ice shelves. The physics that determines the flow of ice is the same for all cases and based on the conservation of mass and momentum and the constitutive equation for ice (Glen's flow law [Glen, 1955]), however, the boundary conditions, in particular at the ice base, are very different and therefore the governing terms that determine the flow are different. We consider here the simplest cases of ice sheet, ice stream and ice shelf flow.

#### 2.1.1. Ice Sheet

[14] For the ice sheet flow we use the SIA [Hutter, 1983], which assumes that the horizontal flow is due to vertical

**Table 1.** Summary of Used Numerical Models for Grounding Line (GL) Migration, With Citations Where Appropriate

Name	Short Description	Type of Grid	Coupling at GL	GL Treatment
<i>Fixed Grid Models</i>				
FGSHSF	sheet shelf, <i>Huybrechts</i> [1990], <i>Ritz et al.</i> [2001]	fixed grid	no mechanical coupling, coupling only through flux and thickness evolution	flotation condition
FGSTSF	stream shelf	fixed grid	full mechanical coupling	flotation condition
<i>Moving Grid Models</i>				
MGSHXX	sheet, <i>Hindmarsh and LeMeur</i> [2001]	moving grid	no coupling (no shelf)	GL migration equation
MGSHSF	sheet shelf	moving grid	no mechanical coupling, only through flux at GL	GL migration equation
MGSTSF	stream shelf	moving grid	full mechanical coupling	GL migration equation

shearing alone. Assuming no sliding at the bed the vertically averaged horizontal velocity  $u$  is given by

$$u = C \left( \frac{\partial s}{\partial x} \right)^n h^{n+1}, \quad (2)$$

where  $s$  is the surface elevation,  $n$  the flow law exponent in Glen's flow law and the constant  $C$  is given by

$$C = \frac{2A(\rho_i g)^n}{n+2}, \quad (3)$$

where  $A$  is the rate factor,  $\rho_i$  the density of ice and  $g$  the acceleration due to gravity.

### 2.1.2. Ice Shelf

[15] The governing equation for an ice shelf that is allowed to spread unidirectionally along the  $x$  axis is given by

$$2 \frac{\partial}{\partial x} h \nu \frac{\partial u}{\partial x} = \rho_i g h \frac{\partial s}{\partial x}, \quad (4)$$

where  $\nu$  is the vertically averaged effective viscosity

$$\nu = A^{-1/n} \dot{\epsilon}^{(1-n)/n} = A^{-1/n} \left[ \left( \frac{\partial u}{\partial x} \right)^2 \right]^{(1-n)/(2n)}, \quad (5)$$

and  $\dot{\epsilon}$  is the vertically averaged effective strain rate given by  $\dot{\epsilon} = |\partial u / \partial x|$ .

### 2.1.3. Ice Stream

[16] For an ice stream, we modify equation (4) by adding a resistance from the bed which is assumed to be linearly related to the velocity  $u$  at the bed (a viscous till is assumed). The equation determining the vertically averaged ice stream velocity  $u$  is then

$$2 \frac{\partial}{\partial x} h \nu \frac{\partial u}{\partial x} - \beta^2 u = \rho_i g h \frac{\partial s}{\partial x}, \quad (6)$$

where  $\beta^2$  is a friction coefficient to be specified. Equation (6) indicates that the driving stress on the right-hand side is balanced by basal traction and longitudinal stress gradients alone. Equations (4) and (6) both ignore lateral resistance to flow, which is thought to be particularly important for ice streams [Whillans and Van der Veen, 1997]. However, we do not regard this as important for the purposes of our study

for three main reasons. First, *Van der Veen and Whillans* [1996] propose a parameterization of lateral resistance in terms of ice stream width  $W$  and velocity  $u$  given by

$$2 \frac{\partial}{\partial x} h \nu \frac{\partial u}{\partial x} - \beta^2 u - \frac{h}{W} \left( \frac{5u}{2AW} \right)^{1/3} = \rho_i g h \frac{\partial s}{\partial x}. \quad (7)$$

By omitting the lateral resistance we implicitly include a linearized version (with constant width) of this parameterization subsumed within the resistance of the bed. Second, this study is focussed on large ice shelves, such as the major present-day Ronne-Filchner and Ross ice shelves as well as the former outer shelves fringing Antarctica, for which lateral drag is expected to be small. Third, the main purpose of the stream shelf model is to investigate the influence of the longitudinal stress coupling on the migration of the grounding line. We select a low value for the basal resistance of  $\beta^2 = 1.0 \times 10^9 \text{ Pa s m}^{-1}$  which is consistent with values found for the Siple coast ice streams [MacAyeal et al., 1995].

### 2.1.4. Boundary Conditions

[17] The ice sheet is assumed to be symmetric at the ice divide, which implies that  $\partial s / \partial x = 0$  and the horizontal flux is zero at the divide ( $\partial q / \partial x = 0$ ). At the shelf-ocean boundary the longitudinal stress is balanced by the hydrostatic pressure of the ocean water. Using Glen's flow law and assuming no spreading to the sides, the boundary condition at the shelf front is given by [Paterson, 1994, p. 296]

$$\left. \frac{\partial u}{\partial x} \right|_{\text{shelffront}} = A \left[ \frac{1}{4} \rho_i g \left( 1 - \frac{\rho_i}{\rho_w} \right) \right]^n h^n, \quad (8)$$

where  $\rho_w = 1028 \text{ kg m}^{-3}$  is the density of the ocean water.

## 2.2. Numerical Models

[18] The two sets of numerical models that are used to solve the equations above differ mainly in the way the grounding line is treated and consequently the kind of grid that is used. The models are described below and an overview is given in Table 1. We refer to the various models using six-letter acronyms (see Table 1), in which the first two characters (FG = fixed grid/MG = moving grid) refer to the type of grid, the second two to the grounded ice model (SH = sheet/ST = stream) and the

third two to the floating ice model (XX = no shelf/SF = shelf).

### 2.2.1. Fixed Grid Models

[19] The first set of models is based on a fixed horizontal grid and the flotation condition is used to decide where the ice is grounded or is part of the shelf, which is given by

$$\rho_i h = \rho_w (l - b), \quad (9)$$

where  $\rho_i$  and  $\rho_w$  are the densities of ice and water respectively,  $l$  is sea level and  $b$  is the elevation of the ice sheet base. The grounding line position is therefore not defined explicitly but must fall between grid points where ice is grounded and floating. This method has been used in large ice sheet models to calculate the migration of the grounding line [Ritz *et al.*, 2001; Huybrechts and De Wolde, 1999; Huybrechts, 1990]. We apply the fixed grid model to two different flow regimes in the grounded part: (1) an ice sheet (equation (2), denoted as FGSFSF model) and (2) an ice stream (equation (6), denoted as FGSTSF model) both with an ice shelf attached to it.

[20] In case of the FGSFSF model, at the last grounded point the horizontal flux is given as input to the ice shelf part of the model. This means no explicit mechanical coupling between ice sheet and ice shelf is considered at the grounding line, however the ice shelf evolution can modify inland ice by the mechanism of geometry change through the thickness evolution equation (equation (1) [Ritz *et al.*, 2001]). For modeling the Antarctic ice sheet, Huybrechts [1990, 1992] considered mechanical coupling at the grounding line by incorporating a decrease in ice viscosity induced by longitudinal stresses at the grounding zone to evaluate the fluxes there. However, in his model this zone is represented only by the last grounded grid cell and the way it is included appears to be fairly arbitrary. Additional model calculations with such a scheme showed (at least for 2D plane flow) no significant difference to our simple mechanically uncoupled model. Thus we assume that the FGSFSF model represents the currently existing and applied ensemble of fixed grid ice sheet models that use the flotation condition (equation (9)) to predict grounding line changes [Huybrechts, 2002; Ritz *et al.*, 2001; Huybrechts and De Wolde, 1999; Huybrechts, 1992, 1990]. The relevant equations are solved numerically using finite differences. In general centered differences are used and the velocities and fluxes are calculated on a staggered grid (see Appendix B). The ice shelf equation (4) and ice stream equation (6) are solved by iterating for the effective viscosity  $\nu$ . For the thickness evolution (equation (1)), an explicit forward time-stepping scheme is used with a constant time step  $\Delta_t$ .

### 2.2.2. Moving Grid Models

[21] The second set of models is based on a moving grid which allows the grounding line position to be followed continuously and uses an expression for the grounding line migration rate to compute the grounding line motion. Following Hindmarsh [1996], from a total differentiation of the flotation condition (equation (9)) the grounding line migration rate  $\dot{L}_g$  is given by

$$\dot{L}_g = \frac{dL_g}{dt} = \frac{\rho_w}{\rho_i} \frac{\partial f}{\partial t} + \frac{\partial q}{\partial x} - a, \quad (10)$$

$$\frac{\partial h}{\partial x} - \frac{\rho_w}{\rho_i} \frac{\partial f}{\partial x}$$

where all quantities are evaluated at the grounding line position,  $L_g$  is the distance of the grounding line from the ice divide and  $f = l - h$  is the water depth at the grounding line. The ice divide is located at  $x = 0$  and the grounding line at  $x = L_g$ .

#### 2.2.2.1. MGSXXX Model

[22] The first moving grid model only considers a grounded ice sheet and ignores any coupling to an ice shelf (noted as MGSXXX). The model has been described and applied by Hindmarsh [1996], Hindmarsh and LeMeur [2001], and LeMeur and Hindmarsh [2001], and dynamical consistency has been shown to exist between the governing equations and the corresponding discretized (finite difference) approximation [Hindmarsh, 1996]. In particular, this means that the numerical model can exhibit neutral equilibria. To accurately compute the motion of the grounding line a normalized horizontal coordinate  $\xi = x/L_g$  is introduced. The position of the ice divide and the grounding line correspond to  $\xi = 0$  and  $\xi = 1$  respectively. A detailed derivation of the surface evolution and grounding line migration equations into the transformed  $\xi$  coordinate system are given in Appendix A.

[23] For the MGSXXX model we follow the discretization scheme suggested by LeMeur and Hindmarsh [2001] and Hindmarsh and LeMeur [2001]. In general, centered finite differences are used except at the grounding line where upstream differences are used for the thickness and surface slope, and the flux divergence (for details of the discretization, see Appendix B).

#### 2.2.2.2. MGSTSF Model

[24] Following the architecture of the MGSXXX model above, an ice stream model that is mechanically coupled to an ice shelf has been developed (noted as MGSTSF). In this case, we follow the shelf front position  $L_{tot}$  as well as the grounding line position. We therefore use a piecewise coordinate transformation and introduce a new coordinate  $\xi$  given by

$$\xi = \begin{cases} \frac{r}{L_g} x & \text{ice sheet : } x \leq L_g \\ \frac{1-r}{L_s} x + \frac{rL_{tot} - L_g}{L_s} & \text{ice shelf : } x > L_g \end{cases}, \quad (11)$$

where  $r$  is the  $\xi$  coordinate of the grounding line position, which is independent of time and is chosen as  $0 < r < 1$  and  $L_s = L_{tot} - L_g$  is the ice shelf length. The ice divide, the grounding line position and the shelf front then correspond to  $\xi = 0$ ,  $\xi = r$  and  $\xi = 1$  respectively (Figure 1). The position of the shelf front in the fixed grid model is fixed, so we chose a fixed shelf front position here as well ( $\partial L_{tot}/\partial t = 0$ ). A detailed formulation of the transformed field and surface evolution equations, and the grounding line migration equation is given in Appendix A.

[25] For the MGSTSF model we tried to follow the discretization scheme of the MGSXXX model, so that in general centered differences are used, except at the grounding line where upstream differences are used again to approximate the thickness and surface slopes, and the flux divergence (for details, see Appendix B). Because the shelf is also modeled we could alternatively use centered differences for the gradients at the grounding line (equation (10)). The sensitivity of the model results on the discretization

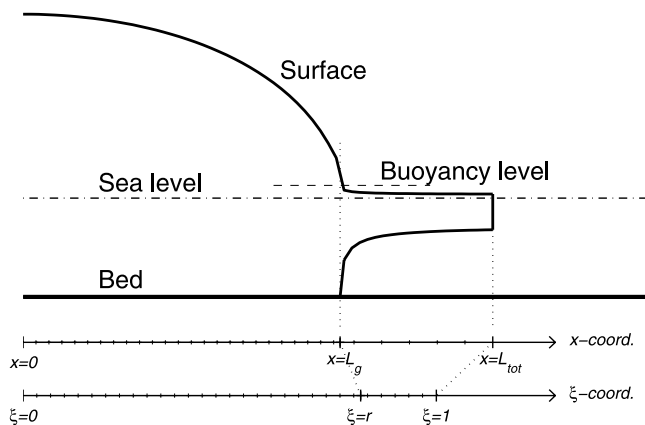


**Figure 1.** Schematic of the two-step coordinate transformation used in the MGSTSF model and in the MGSFSF model:  $x$  and  $\xi$  denote horizontal coordinates of the original grid and the stretched grid, respectively.

scheme (centered or upstream) is therefore explored in a later section. In contrast to the MGSXXX model, the grounding line in this model is on the staggered grid (see details in section B2.2 and Figure B1). This was done to ensure mass conservation over the grounding line.

### 2.2.2.3. MGSFSF Model

[26] A third moving grid model considers an ice sheet coupled only by the flux at the grounding line to an ice shelf. This model employs the same piecewise coordinate transformation as the MGSTSF model, and the grounding line is again on the staggered grid. This model was used to compare the MGSTSF with a model that uses the same discretization scheme but different physics. This MGSFSF model did not give significantly different results to the one using the scheme of the MGSXXX model.

[27] For the thickness evolution in all moving grid models (MGSXXX, MGSTSF and MGSFSF), an explicit forward time-stepping scheme is used with a constant time step  $\Delta t$  (for details, see Appendix B). The thickness evolution scheme used in all models is mass conservative at the grounding line.

[28] Although finite difference schemes are not formally mass conserving at the grounding line, we have checked that mass is indeed conserved in all the fixed and moving grid models above.

## 3. EISMINT Grounding Line Migration Experiments

[29] Although, a few attempts have been made to model grounding line migration, the only comparison of grounding line treatments in numerical models was undertaken in the European Ice Sheet Modelling Initiative (EISMINT) programme [Huybrechts, 1997]. All compared models used a fixed grid and the experiments were restricted to one initial geometry with a ice sheet length of 50 km and a shelf of the same length, and considered the plane flow case. A constant rate factor corresponding to an ice temperature of about  $-34^\circ\text{C}$  was used. This setting appears unrealistic and may not represent the situation of the WAIS (or any large marine ice sheet). However, it is the only known model

comparison for grounding line migration, so we base the first set of model experiments on the EISMINT setup. Here we apply the ice sheet/shelf models (FGSHSF and MGSXXX) and compare the results with the EISMINT comparison study.

### 3.1. Model Setup and Model Parameters

[30] Following EISMINT, we consider an ice sheet of 50 km initial length with an attached ice shelf of another 50 km (Figure 2). The initial grid spacing in the  $x$  direction is 2 km resulting in 51 grid points of which the first 26 are on grounded ice. The bed is an inclined plane with a slope of  $-0.005^\circ$  and with an elevation of  $-250$  m at the ice divide and  $-750$  m at the shelf front. The rate factor is  $A = 1.0 \times 10^{-18} \text{ Pa}^{-3} \text{ a}^{-1}$  [Paterson and Budd, 1982].

### 3.2. Experiments

#### 3.2.1. Steady State Calculations

[31] First, a steady state geometry is allowed to develop for an initial accumulation rate of  $0.3 \text{ m a}^{-1}$ . For the FGSHSF model the last grounded grid point is fixed until a steady state is reached and then the grounding line is allowed to freely evolve until a steady state is reached. After relaxing of the initially fixed grounding line, the grounding line position is found to be stable and the geometry does not show any further change. For the MGSXXX model, we start with a numerical steady state solution following *LeMeur and Hindmarsh* [2001]. Allowing this solution to evolve with time showed no change in the geometry, thus this initial geometry is in a real steady state. In Figures 3–6, the first 5 ka show the initialization phase of the steady state for the FGSHSF and the MGSXXX model respectively. The geometry of the steady states (5 ka) which are used as initial geometry for the following experiments are shown in Figure 2. For the grounded part, the steady geometries for both models are almost identical.

#### 3.2.2. Step Change Experiments

[32] Starting from the steady state geometries obtained above, the response of the surface and the grounding line to step changes of the accumulation rate from  $0.3 \text{ m a}^{-1}$  to  $0.5 \text{ m a}^{-1}$  and to  $0.1 \text{ m a}^{-1}$ , respectively, and to sea level changes of  $\pm 125$  m are investigated. In Figures 3–6, these step changes are made at 5 ka. After reaching a new steady

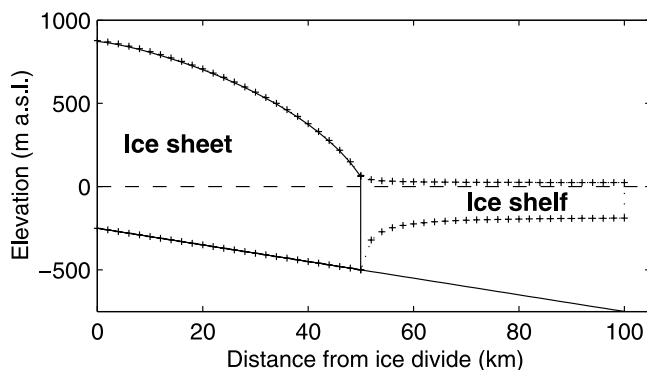


**Figure 2.** Steady state geometry used as initial geometry for the EISMINT experiments. The crosses denote the geometry for the FGSHSF model, and the solid line denotes the geometry for the MGSXXX model.

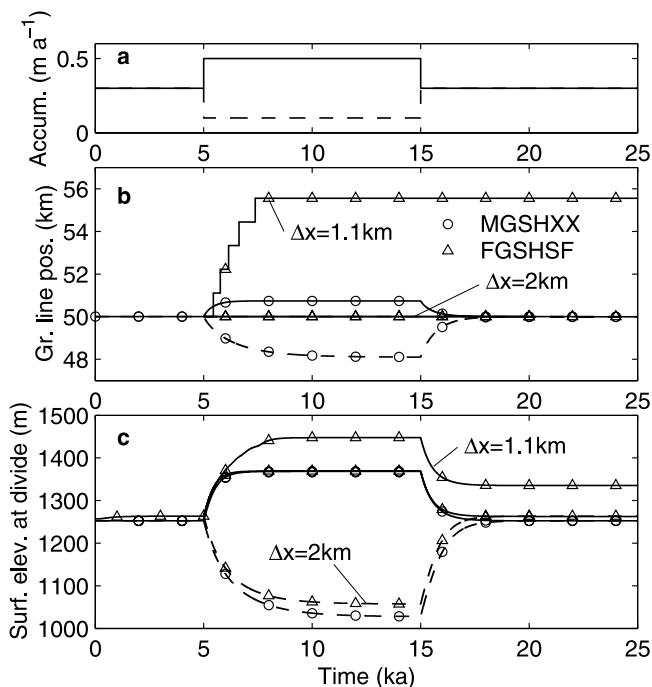


**Figure 3.** Modeled response to a step change of the accumulation rate at time 5 ka from  $0.3 \text{ m a}^{-1}$  to  $0.5 \text{ m a}^{-1}$  (solid lines) or to  $0.1 \text{ m a}^{-1}$  (dashed lines), respectively. At time 15 ka the accumulation rate has been reset to  $0.3 \text{ m a}^{-1}$ . (a) Accumulation rate and (b) grounding line position calculated by the MGSXXX model (circles) and by the FGSHSF model (triangles). Note that for the FGSHSF model, calculations for a higher horizontal grid resolution of  $\Delta_x = 1.1 \text{ km}$  (additionally to  $\Delta_x = 2 \text{ km}$ ) is shown. (c) Elevations at the ice divide with symbols and lines corresponding to Figures 3a and 3b.

state, at 15 ka the accumulation rate or sea level are reset to their initial values of  $0.3 \text{ m a}^{-1}$  and 0 m above sea level respectively, and the model is run for another 10 ka.

**3.2.2.1. Change in Accumulation**

[33] For the FGSHSF model, for a step change in accumulation from  $0.3 \text{ m a}^{-1}$  to  $0.5 \text{ m a}^{-1}$  the grounding line did not advance (Figure 3). However, by increasing the grid resolution from 51 to 91 grid points ( $\Delta_x = 1.1 \text{ km}$  instead of 2 km) for the same experiment the grounding line advanced by about 5.5 km (five grid points) before finding a new

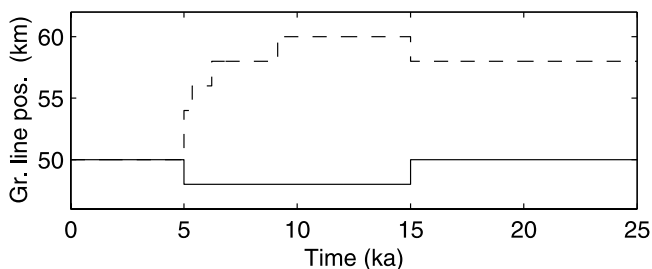


**Figure 4.** Response of the grounding line to a step change in sea level to  $+125 \text{ m a}^{-1}$  (solid lines) and  $-125 \text{ m a}^{-1}$  (dashed lines) calculated with the FGSHSF model. At time 15 ka the sea level has been reset to 0 m.

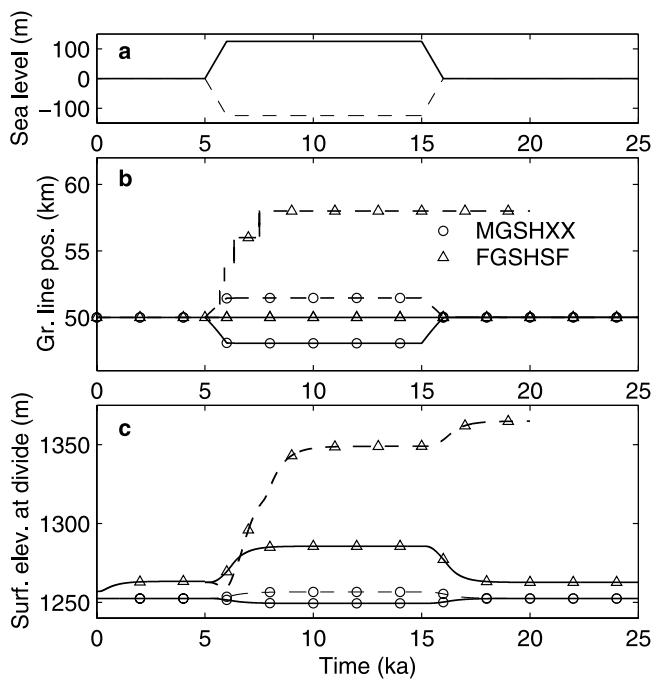


**Figure 5.** Modeled response to a gradual change in sea level over 1 ka to  $+125 \text{ m a}^{-1}$  (solid lines) and  $-125 \text{ m a}^{-1}$  (dashed lines). At time 15 ka the sea level has been gradually reset to 0 m. (a) Sea level and (b) grounding line position calculated by the MGSXXX model (circles) and by the FGSHSF model (triangles). (c) Elevations at the ice divide with symbols and lines corresponding to Figures 5a and 5b.

steady state. This indicates a grid-size dependency which will be discussed in detail in a later section. After switching the accumulation back to its initial value, the grounding line did not retreat in the 91-grid point run. Hence the change in

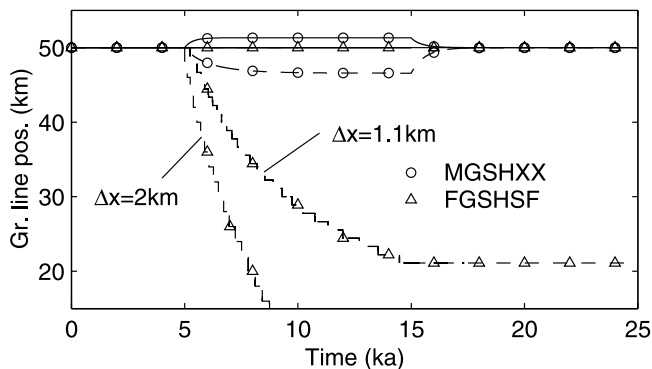


**Figure 6.** Modeled response to a step change of the accumulation rate at time 5 ka to  $0.5 \text{ m a}^{-1}$  (solid lines) and  $0.1 \text{ m a}^{-1}$  (dashed lines), respectively. At time 15 ka the accumulation rate has been reset to  $0.3 \text{ m a}^{-1}$ . Here a rate factor  $A$  corresponding to an ice temperature of  $-15^\circ\text{C}$  is used. The circles indicate the grounding line position calculated by the MGSXXX model, and the triangles indicate the grounding line position calculated by the FGSHSF model. Note that for the FGSHSF model the grounding line position for a higher horizontal grid resolution of  $\Delta_x = 1.1 \text{ km}$  is also shown.

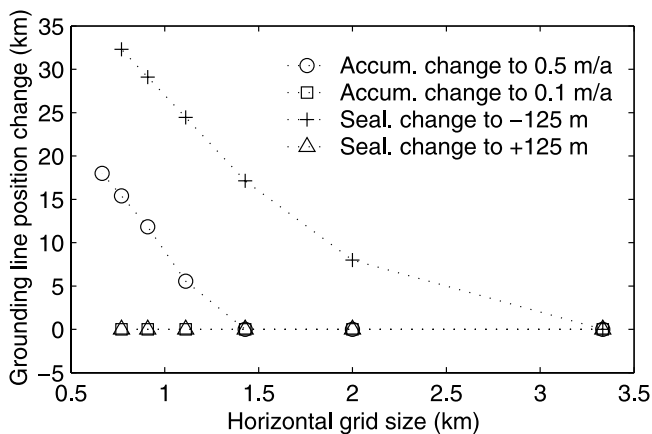


**Figure 7.** Total grounding line change after reaching a steady state calculated with the FGSHSF model shown against horizontal grid size for the different labeled perturbation experiments.

grounding line position in this experiment appears to be irreversible. For the experiment with a decrease in accumulation rate to  $0.1 \text{ m a}^{-1}$ , no retreat is observed for the FGSHSF model (Figure 3). An increase in grid resolution here did not change the result.

[34] For the MGSXXX model, results are distinctly different (Figure 3). As demonstrated by *Hindmarsh* [1996] and *Hindmarsh and LeMeur* [2001], for any kind of change in accumulation the grounding line migrates and after resetting accumulation, the grounding line goes back to its original position. Thus here we have a reversible system. There seems to be no indication that an advance is preferred over a retreat. The magnitude of grounding line change is in the order  $\pm 1 \text{ km}$  and is small relative to the changes obtained from the FGSHSF model (in the cases where a change has occurred).

### 3.2.2.2. Change in Sea Level

[35] For a step change in sea level to  $\pm 125 \text{ m}$  the results are shown in Figure 4. For a rise of sea level, the FGSHSF model shows an immediate retreat of the grounding line, but only by one grid point (2 km). After resetting sea level to zero it readvances back to its initial position. For a decrease in sea level to  $-125 \text{ m}$ , the grounding line advances by five grid points (10 km) and after resetting sea level to 0 m the grounding line only retreats by one grid point and does not go back to the initial position.

[36] A step change in sea level does not occur in reality and is an unsuitable experiment for the MGSXXX model because the calculation of the grounding line migration rate (equation (10)) explicitly uses the water depth changing rate  $\partial f / \partial t$  which is infinite in case of a step sea level change. Therefore in the further experiments, we apply a gradual change of sea level by  $\pm 125 \text{ m}$  over a period of 1 ka (Figure 5a).

[37] The results for a gradual change in sea level over 1 ka for the FGSHSF model (Figure 5) are qualitatively very similar to the step change experiment (Figure 4). The only difference is that, in the case of sea level rise, the grounding line does not retreat and the increase in sea level only results in a thickening of the grounded part.

[38] For the MGSXXX model, a gradual rise of the sea level to  $+125 \text{ m}$  results in a retreat of the grounding line of 2 km and for a sea level lowering the grounding line advances by 1.5 km (Figure 5). Again the total amount of grounding line change is small relative to the changes of the FGSHSF model, if they occur at all. For both cases, after resetting sea level to 0 m at 15 ka (or at any other time) the grounding line position goes back to its initial value.

[39] Note that a realistic timescale for sea level changes of this order of magnitude is 10 ka, as occurred at the transition from the Last Glacial Maximum to the Holocene. Our sea level change experiment is therefore fairly extreme, but it allows a comparison to the step change experiments in the EISMINT study. Furthermore, additional calculations with a gradual change of sea level to  $\pm 125 \text{ m}$  over a period of 10 ka, show the same results for total amount of change in geometry and grounding line position, although the timing is different.

### 3.2.2.3. Sensitivity to Rate Factor

[40] The chosen value of  $A = 1.0 \times 10^{-18} \text{ Pa}^{-3} \text{ a}^{-1}$  in the EISMINT comparison (corresponding to a temperature of  $-34^\circ\text{C}$ ) is rather too low to be realistic. We therefore repeated the accumulation step change experiment with a rate factor of  $A = 9.2 \times 10^{-18} \text{ Pa}^{-3} \text{ a}^{-1}$  (corresponding to  $-15^\circ\text{C}$ ). The results are shown in Figure 6. The qualitative results for the MGSXXX model are very similar to the experiments with the colder ice, although the absolute values of grounding line change are slightly larger. For the FGSHSF model the results are significantly different. For an increase of the accumulation rate to  $0.5 \text{ m a}^{-1}$ , the grounding line does not advance even for increased grid resolution up to  $\Delta_x = 0.67 \text{ km}$  (151 grid points) instead of 2 km (51 grid points). For a decrease of the accumulation rate to  $0.1 \text{ m a}^{-1}$ , the grounding line starts to retreat very rapidly and the ice sheet disappears completely after 5 ka years, although the retreat rate decreases toward the end. For an increased horizontal grid resolution of  $\Delta_x = 1.1 \text{ km}$  (instead of 2 km), the retreat is much slower and the grounding line reaches a steady state position which is about two thirds of its initial position. Thus in contrast to the tendency to advance shown in the previous EISMINT case, a retreating tendency is observed.

### 3.2.3. Sensitivity to Time Step and Grid Size

[41] For both models, the sensitivity of the results to the grid size and time step was also investigated. Experiments with an accumulation step change to  $0.1 \text{ m a}^{-1}$  or to  $0.5 \text{ m a}^{-1}$  or a gradual sea level change to  $\pm 125 \text{ m}$  over 1 ka were performed for time steps between 5.0 and 0.1 years, and horizontal grid sizes between 3.33 km and 0.77 km (corresponding to 31–131 grid points along the domain). As indicated above the amount of grounding line change obtained by the FGSHSF model strongly depends on the horizontal grid size (Figure 7). For large grid sizes and small perturbations, no advance or retreat of the grounding line occurs. If any advance occurs, the amount of advance increases with decreasing grid size. This grid size dependency seems to be mainly a consequence of using a fixed grid. Whenever the grid is too sparse, thickening (or thinning) around the grounding line is not high enough to allow the first shelf grid point to become grounded (or the last grounded grid point to float). The grounding line is therefore unable to change and is tied to its initial position.

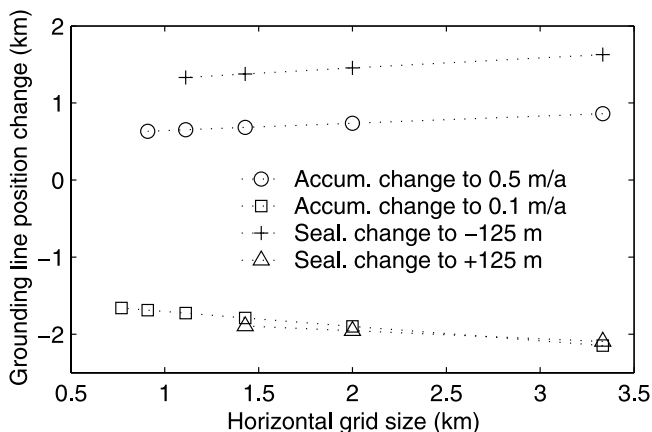


**Figure 8.** Total grounding line change after reaching a steady state calculated with the MGSXX model shown against initial horizontal grid size for the different labeled perturbation experiments.

[42] For the MGS model we also observe a dependency of grounding line change on the chosen horizontal grid size (Figure 8), however, the dependency is weak and significantly smaller than the grid size and therefore within the accuracy of the model. Furthermore, the change in grounding line position decreases with decreasing grid size.

[43] All experiments were repeated with varying time steps between 5.0 and 0.1 years. For both models, the calculated response was the same once the time step was small enough to be stable for the current grid size (Courant condition [Press *et al.*, 1992, p. 829]).

### 3.3. Summary of the EISMINT Experiments

[44] In case of the FGSHSF model, grounding line changes (where a change occurs) are in the order of several grid points (5–10 km) and a tendency to advance rather than retreat is observed. Furthermore, the perturbation experiments are found to be irreversible. This hysteresis of the grounding line position, the magnitude of grounding line change and the tendency to advance are consistent with the results of the fixed grid models of the EISMINT comparison study [Huybrechts, 1997]. This supports our contention that the FGSHSF model is representative of the current generation of fixed grid ice sheet models.

[45] A new result from our model experiments is that the dynamics of the grounding line resulting from the FGSHSF model is strongly affected by the ice rheology (i.e., assumed ice temperature) and by the chosen horizontal grid size. The latter is crucial, because it implies that the predictions of fixed grid models for the evolution of marine ice sheets are not independent of the models' numerics. In the EISMINT comparison study the dependency on numerics or rheology was not investigated.

[46] The results from the MGSXX model are qualitatively very different. For any external forcing, the grounding line changes and finds a new steady state position, but the amount of change is in general small (<2 km) and no preference for an advance or retreat is observed. Furthermore, all experiments are reversible. The stable behavior is a characteristic dynamical features of a marine ice sheet with the property of neutral equilibrium. No qualitative

dependency of ice sheet dynamics on ice rheology was observed and the observed small dependency on horizontal grid size is within the accuracy of the numerical model. The chief conclusion from this section is therefore that moving grid models appear to be more robust than fixed grid models, and that the predictions of the latter show strong dependency on numerical details.

## 4. Ice Sheet Experiments

[47] The experiments described above are not representative of the true dimensions and parameter values of a marine ice sheet, therefore we perform a series of model experiments for a more realistic model setting, representing the dimensions of the WAIS. The half width of the grounded part is set to 750 km and the shelf length to 250 km. The whole domain has 81 horizontal grid points, of which initially 61 points are grounded (corresponding to  $\Delta_x = 12.5$  km). The initial water depth at the terminus is 500 m. To investigate the effect of basal topography, three different slopes of  $-0.0006^\circ$ ,  $0.0^\circ$ , and  $+0.0006^\circ$  are chosen for the bedrock topography (see Figure 9). The rate factor of  $A = 1.4 \times 10^{-17} \text{ Pa}^{-3} \text{ a}^{-1}$  (corresponding to  $-10^\circ\text{C}$ ) is used, a value often used for modeling ice sheets [Paterson, 1994, p. 97]). An initial accumulation rate of  $0.2 \text{ m a}^{-1}$  is used here. We will explicitly note when different parameters or geometries are used.

[48] The model experiments are similar to those performed for EISMINT. In a first phase initial steady states are calculated for the parameter setting described above. Using these steady states as initial geometries, the response of the marine ice sheet to step changes in accumulation to  $0.1 \text{ m a}^{-1}$  and  $1.0 \text{ m a}^{-1}$ , and gradual changes of sea level to  $\pm 125 \text{ m}$  over a period of 10 ka years are calculated. Occasionally, a shorter period of 1 ka has been chosen for the sea level change experiments to reduce computation time, however, the results for these cases are qualitatively very similar although the timing is different. The results for the ice sheet experiments are summarized in Figures 10–15.

### 4.1. MGSXX Model

[49] In general, the results of the MGSXX model are qualitatively the same as those from the EISMINT experi-

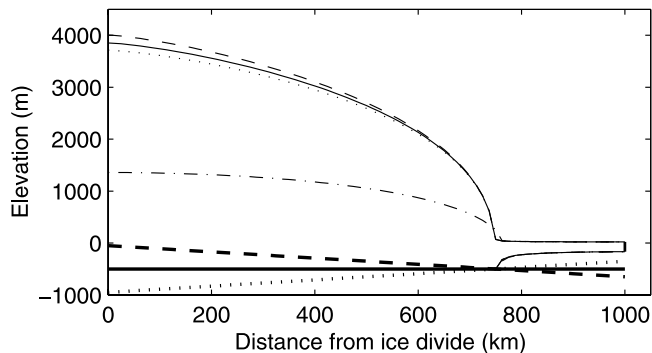


**Figure 9.** Initial steady state ice sheet and shelf geometries for the three different ice sheet base slopes: flat (solid lines), down sloping (dashed lines), and up sloping base (dotted lines). The dash-dotted line shows the initial surface steady state for the ice stream (MGSTSF model) for a flat bed.

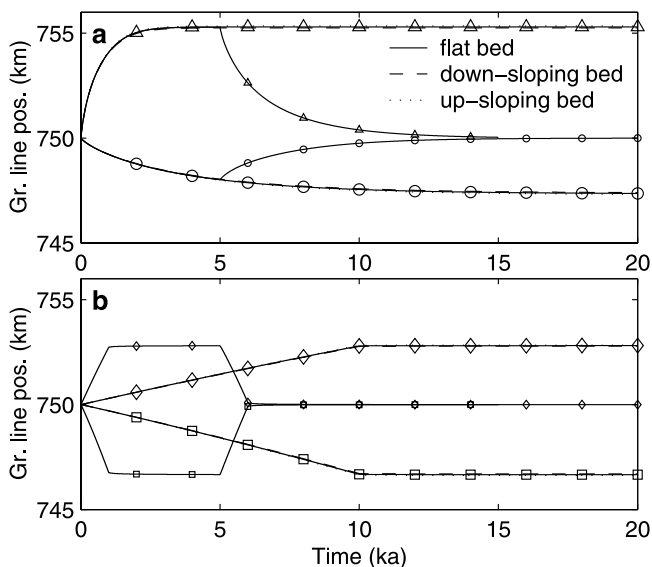


**Figure 10.** Response of the grounding line to different perturbation experiments calculated with the MGSXXX model. The solid, the dashed, and the dotted lines refer to a flat, down sloping, and up sloping ice sheet base, respectively. (a) Circles and triangles refer to a step change in accumulation to  $0.1 \text{ m a}^{-1}$  and  $1.0 \text{ m a}^{-1}$ , respectively. The small symbols refer to experiments where the accumulation rate has been reset to the initial value at 5 ka. (b) Diamonds and squares refer to a gradual change of sea level to  $-125 \text{ m}$  and  $+125 \text{ m}$ , respectively, over a period of 10 ka. The small symbols refer to the same changes but over a period of 1 ka, and sea level has been reset to 0 m at 5 ka.

ments. For any forcing in accumulation rate or sea level, the grounding line changes and finds a new steady state position (Figure 10). Again, the amount of grounding line change is small relative to the ice sheet length (below 1% (Table 2)). As expected, the relative thickness change is more pronounced in the accumulation change experiment, while in the sea level change experiment the surface geometry remains almost constant (Table 2). After switching back the external forcing to its initial value, the ice sheet goes back to its initial state, which means the perturbation experiments are reversible. These findings are independent of the basal topography chosen (Figure 10) as previously demonstrated in detail by *LeMeur and Hindmarsh* [2001]. Also, the amount of grounding line change is almost independent of the basal topography (Table 2). Results for the same experiments with the MGSFSF model, that couples an ice sheet to the shelf through the flux at the grounding line (grounding line is on staggered grid), are quantitatively and qualitatively very similar to the results from the MGSXXX model.

#### 4.2. FGSHSF Model

[50] For the FGSHSF model, a reduction in accumulation to  $0.1 \text{ m a}^{-1}$  or an increase in sea level to 125 m leads to a significant retreat of the grounding line position (Figure 11). In contrast, even a large increase in accumulation to  $2.0 \text{ m a}^{-1}$  or a sea level lowering to  $-250 \text{ m}$  does not cause an advance. This is in contrast to the preference for advance

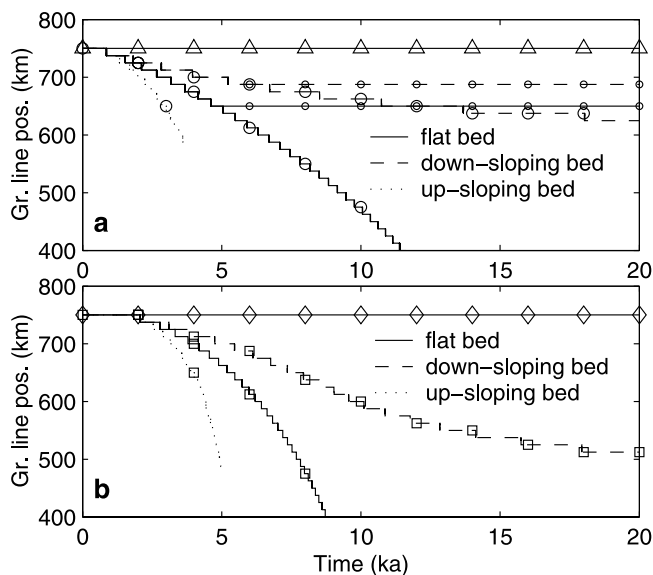


**Figure 11.** Response of the grounding line to different perturbation experiments calculated with the FGSHSF model. The solid, dashed, and dotted lines refer to a flat, down sloping, and up sloping ice sheet base, respectively. (a) Circles and triangles refer to a step change in accumulation to  $0.1 \text{ m a}^{-1}$  and  $1.0 \text{ m a}^{-1}$ , respectively. The small symbols refer to experiments where the accumulation rate has been reset to the initial value at 5 ka. (b) Diamonds and squares refer to a gradual change of sea level to  $-125 \text{ m}$  and  $+125 \text{ m}$ , respectively, over a period of 10 ka.

found in the EISMINT experiments. The reason for this is mainly related to the choice of the rate factor within the shelf and is discussed later. For a flat bed, we found that the retreat caused by a reduction in accumulation or an increase in sea level is unstable, and the ice sheet eventually vanishes (Figure 11). Such an unstable response is also obtained for the case of a bed that slopes upward in the direction of flow (as is the case for the WAIS) and the rates of retreat are even higher. In contrast, a down sloping bed leads to a stable

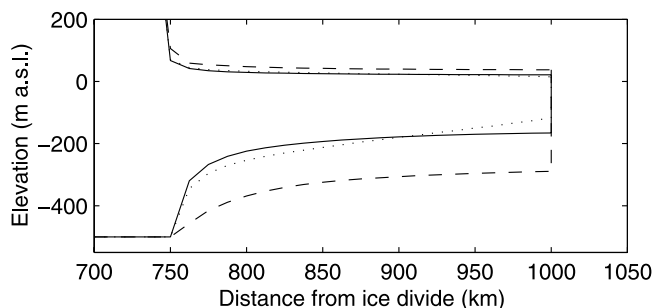


**Figure 12.** Initial steady state geometries of the shelf and the grounding line zone for different parameter settings in the FGSHSF model: rate factor corresponding to  $-10^\circ\text{C}$  (solid lines), rate factor corresponding to  $-30^\circ\text{C}$  within the shelf (dashed lines), and rate factor corresponding to  $-10^\circ\text{C}$  but additionally considering lateral drag by equation (12) (dotted lines).

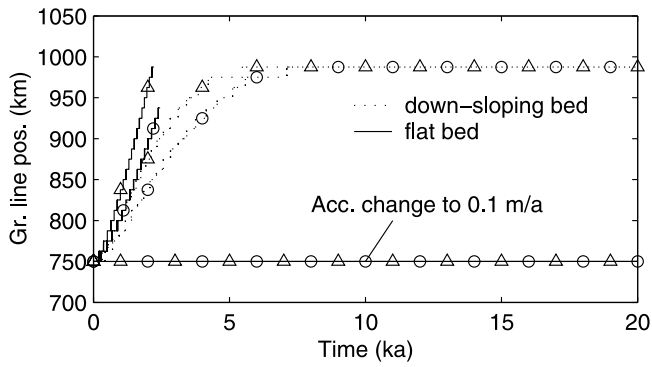


**Figure 13.** Response of the grounding line to a step change in accumulation to  $1.0 \text{ m a}^{-1}$  calculated with the FGSHSF model. Here the case of a higher rate factor corresponding to  $-30^\circ\text{C}$  instead of  $-10^\circ\text{C}$  within the ice shelf (circles) and the whole ice domain (triangles) are shown. No change is observed for a step change in accumulation to  $0.1 \text{ m a}^{-1}$  (as labeled).

retreat of the grounding line which eventually attains new steady state. Note that for this down sloping, “stable” case, the grounding line change is  $-137.5 \text{ km}$  for an accumulation change  $0.1 \text{ m a}^{-1}$  and  $-237.5 \text{ km}$  for the change in sea level to  $+125 \text{ m}$ , which is one to two orders of magnitude higher than for the MGSXXX model (Table 2).

[51] After switching back the external forcing to the initial value at 5 ka, the grounding line (whenever a change has occurred) does not go back to its initial position (Figure 11a). In contrast to the MGSXXX model, the perturbation experiments are again not reversible with this model.

**4.2.1. Sensitivity to Rate Factor**

[52] The preference for retreat over advance in the FGSHSF model (Figure 11) is expected to be mainly a consequence of the higher rate factor employed in this set of experiments. This was already indicated in the EISMINT experiment when repeated with a higher rate factor. In the ice shelf, a higher rate factor corresponds to a lower effective viscosity and leads to enhanced longitudinal extension rates, and therefore to a generally thinner ice shelf

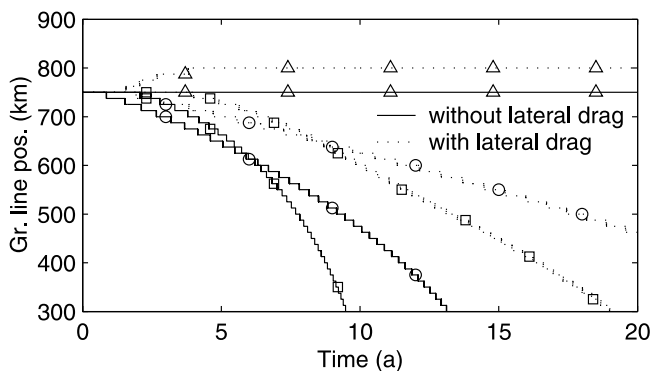


**Figure 14.** Response of the grounding line calculated with the FGSHSF model with (dotted lines) or without (solid line) consideration of lateral drag to different perturbation experiments: a change in sea level to  $+125 \text{ m}$  (squares), a change in accumulation to  $0.1 \text{ m a}^{-1}$  (circles) and  $1.0 \text{ m a}^{-1}$  (triangles). All experiments are for a flat ice sheet base.

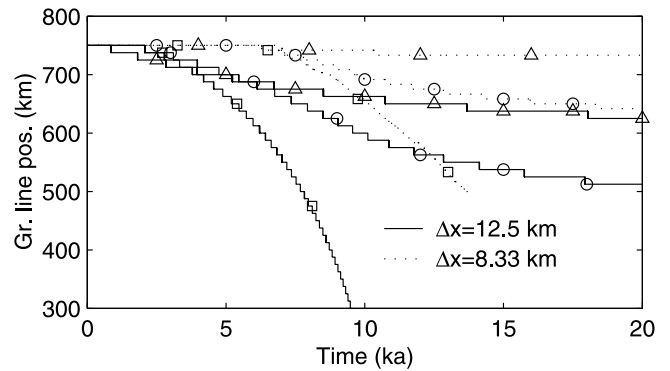


**Figure 15.** Response of the grounding line calculated with the FGSHSF model and a down sloping bed to a decrease in accumulation to  $0.1 \text{ m a}^{-1}$  (triangles) and an increase in sea level to  $+125 \text{ m}$  over 10 ka (circles) for two different grid sizes ( $\Delta x = 12.5 \text{ km}$ , solid lines;  $\Delta x = 8.33 \text{ km}$ , dotted lines). The squares show the sea level change experiment for the case of a flat base.

and a stronger thickness gradient immediately down glacier of the grounding line (Figure 12). As a consequence, for the first grid point downstream from the grounding line to become grounded and the grounding line to advance, a much larger change in flux is needed. Experiments with a rate factor corresponding to  $-10^\circ\text{C}$  in the sheet and  $-30^\circ\text{C}$  in the shelf show that an advance is now obtained for an increase in accumulation to  $1.0 \text{ m a}^{-1}$  (Figure 13). An even faster advance is obtained when a rate factor corresponding to  $-30^\circ\text{C}$  is used for the whole domain. On the other hand, retreat cannot now be generated even for a decrease in accumulation to  $0.01 \text{ m a}^{-1}$ . In contrast, MSSHXX model experiments with a higher rate factor did not significantly change the response of the grounding line.

[53] This type of rate factor dependency in the FGSHSF model also occurs for the sea level increase experiment, and implies that in a fixed grid model the choice of the rate factor and therefore the temperature within the shelf

**Table 2.** Change in Grounding Line ( $\Delta L_g$ ) and in Surface Elevation at the Ice Divide ( $\Delta s_d$ ) for Different Basal Slopes and the Two Ice Sheet Models MGSXXX and FGSHSF<sup>a</sup>

$a_+$ , $\text{m a}^{-1}$	$l_+$ , m	Basal Slope	MGSXXX		FGSHSF	
			$\Delta L_g$ , %	$\Delta s_d$ , %	$\Delta L_g$ , %	$\Delta s_d$ , %
<i>Accumulation Change</i>						
0.1	flat		-0.35	-8.4	$-\infty$	...
0.1	up		-0.36	-7.8	$-\infty$	...
0.1	down		-0.35	-8.9	-18.33	-16.1
1.0	flat		0.71	22.6	0	22.2
1.0	up		0.70	24.2	0	20.7
1.0	down		0.71	21.5	0	23.9
<i>Sea Level Change</i>						
+125	flat		-0.44	-0.10	$-\infty$	...
+125	up		-0.45	-0.10	$-\infty$	...
+125	down		-0.43	-0.09	-31.7	-15.4
-125	flat		0.37	0.11	0	-0.06
-125	up		0.38	0.12	0	-0.07
-125	down		0.37	0.10	0	-0.06

<sup>a</sup>The performed experiments are accumulation step changes to  $a_+$  and sea level changes to  $l_+$ . A response of  $-\infty$  means an unstable retreat.

**Table 3.** Change in Grounding Line ( $\Delta L_g$ ) Calculated by the MGSXXX Model for Different Initial Horizontal Grid Sizes ( $\Delta_x$ ) for a Down Sloping Bed<sup>a</sup>

$a_+$ , m a <sup>-1</sup>	$l_+$ , m	$\Delta_x$ , km	$\Delta L_g$	
			km	%
<i>Accumulation Step Change</i>				
0.1		8.33	-2.11	-0.28
0.1		12.5	-2.60	-0.35
0.1		25.0	-3.93	-0.52
1.0		8.33	4.15	0.55
1.0		12.5	5.33	0.71
1.0		25.0	8.26	1.10
<i>Sea Level Change</i>				
	+125	8.33	-2.93	-0.39
	+125	12.5	-3.31	-0.43
	+125	25.0	-4.23	-0.56
	-125	8.33	2.39	0.32
	-125	12.5	2.78	0.37
	-125	25.0	3.72	0.49

<sup>a</sup>The performed experiments are accumulation step changes to  $a_+$  and sea level changes to  $l_+$ .

strongly affects qualitative predictions of grounding line migration. Using a model which includes mechanical coupling at the grounding line, *Huybrechts and De Wolde* [1999] and *Huybrechts* [2002] similarly found that the evolution of the Antarctic ice sheet was sensitive to the treatment of temperature within the ice shelf. Here we show that such a shelf temperature sensitivity is independent of any mechanical coupling between the grounded and floating ice.

[54] We also found that a lower rate factor in the shelf does not affect the qualitative dependency of grounding line change on basal topography (Figure 13). All experiments with this model exhibited an unstable advance for the case of a flat or up sloping bed, and a stable advance toward a steady state for the case of a down sloping bed.

#### 4.2.2. Effect of Lateral Drag in the FGSHSF Model

[55] The shelf in the FGSHSF model spreads freely in the direction of flow, thus no resistance from the sides is considered. Most real ice shelves are confined to the sides and therefore encounter resistive forces. Although in the case of large ice shelves these back stresses are expected to be small, they may have a stabilizing effect on the grounding line migration. Therefore some model experiments are repeated with a model that accounts in a simple way for lateral stress gradients by adding a term in the stress balance (equation (4)) which is linearly related to the horizontal flow velocity and ice thickness [*Van der Veen and Whillans*, 1996]:

$$\gamma \cdot u(x)h(x), \quad (12)$$

where  $\gamma$  controls the resistance from the sides and is set to  $\gamma = 2 \times 10^4$  Pa s m<sup>-2</sup>, a value that corresponds to an ice shelf width of roughly 1000 km and is appropriate to the Ross or Ronne-Filchner ice shelves. The effect of lateral drag on the shelf geometry and grounding line migration is illustrated in the Figures 12 and 14. In contrast to the case without lateral drag, an advance is now obtained for a change of accumulation to 1.0 m a<sup>-1</sup> with a flat bed, and furthermore the advance is now stable. For a decrease in

accumulation or increase in sea level, the retreat is slower in the case of a flat bed, however the retreat still appears to be unstable. Thus the inclusion of lateral drag seems to have a stabilizing effect on grounding line motion and may also weaken the preference for retreat over advance. Hence in a three-dimensional version of a fixed grid marine ice sheet model (which implicitly includes flow resistance from the side), the observed instability for a flat or up sloping base, as well as the tendencies for retreat or advance, are all expected to be reduced. Because the MGSXXX model does not consider a shelf the effect of lateral drag within the shelf was not investigated.

#### 4.3. Sensitivity to Horizontal Grid Size

[56] As already seen in the EISMINT experiments, the results from the FGSHSF model in this configuration strongly depend on the grid size. For a step change in accumulation to 0.1 m a<sup>-1</sup>, a grid size of 8.33 km (121 grid points) instead of 12.5 km (81 grid points) leads to a slower retreat for a flat bed (Figure 15). As for the sea level increase experiment to +125 m, the advance slows for a smaller grid sizes. For a down sloping bed, the retreat rates and the total retreat of the grounding line decrease with decreasing grid size. Including lateral drag in the shelf (see above) did not remove the grid-size dependency of the FGSHSF model. In contrast, as in the EISMINT experiments, the MGSXXX model is only slightly dependent on the grid size and this dependency is within the resolution of the model (Table 3).

#### 4.4. Summary of Ice Sheet Experiments

[57] The qualitative dynamics of both models with a down sloping bed is the same as in the EISMINT case. The one exception is that there is tendency for retreat in the FGSHSF model rather than advance, which is a result of the higher rate factor employed in these experiments. The strong dependency on ice rheology in fixed grid models implies that an accurate computation of temperature within the shelf and in the grounding line region is needed for the accurate modeling of grounding line migration.

[58] The experiments for different basal slopes show that the results from the MGSXXX model are qualitatively unaffected by the slope of the bed, whereas dynamics of the grounding line in the FGSHSF model strongly depend on basal topography. For a down sloping bed, a change in sea level or accumulation leads to a stable advance or retreat that reaches a new steady state, however for a flat or up sloping bed (which has not been considered in the EISMINT study [*Huybrechts*, 1997]), we observe an accelerated, unstable advance or retreat. This would imply that in the case of the WAIS, once the grounding line starts to retreat, it would not stop until it reaches a down sloping bed. Similarly, once the grounding line starts to advance, it would not stop until it reaches the outer edge of the continental shelf (where it would encounter much deeper water). The observed instability also indicates that this model does not exhibit stable neutral equilibria. The incorporation of lateral drag within the shelf is observed to weaken the instability, but it does not seem to remove it. Whether such an instability can occur in reality has not yet been shown from field observations and is difficult to prove theoretically. It should be stressed here that only the fixed

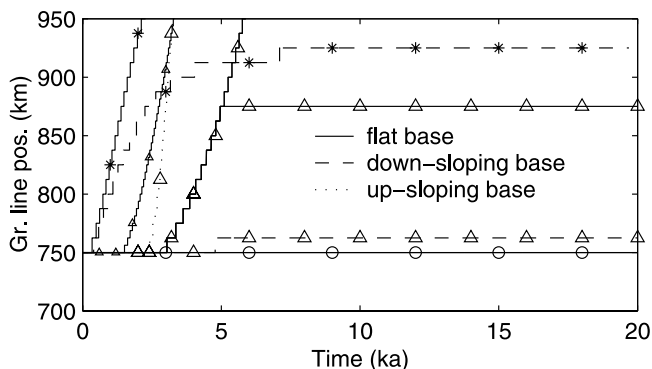


**Figure 16.** Response of the grounding line calculated with the FGSTS model to a change in accumulation to  $1.0 \text{ m a}^{-1}$  (triangles) and  $0.1 \text{ m a}^{-1}$  (circles) for a flat base (solid lines), an up sloping base (dotted lines), and a down sloping base (dashed lines). For the accumulation change experiment to  $1.0 \text{ m a}^{-1}$  the grounding position is also shown for the case of a switch back of the accumulation after 5 ka to the initial value. The small triangles refer to the accumulation change experiment to  $1.0 \text{ m a}^{-1}$  with a flat base but a smaller horizontal grid size of 6.25 km instead of 12.5 km, as before. The stars show the accumulation change experiment to  $1.0 \text{ m a}^{-1}$  considering lateral drag.

grid model exhibits unstable behavior, and that the moving grid models exhibit the type of stable neutral equilibria postulated by *Hindmarsh* [1996].

[59] A further crucial result is that the results of the FGSHSF model are again strongly affected by the grid size and therefore by the numerics, independent of basal topography, rate factor or lateral drag.

## 5. Ice Stream Experiments

[60] In this section, we investigate the influence on grounding line migration of mechanical coupling between the grounded ice and the shelf. For the grounded component we use the ice stream model, and we attached it to an ice shelf. Again a fixed grid model (named FGSTS) and a moving grid model (named MGSTS) are used (Table 1). Both models consider momentum coupling (mechanical coupling) over the grounding line. The equations for ice stream flow (equation (6)) and ice shelf flow (equation (4)) are solved simultaneously for both models by iterating for the effective viscosity given by equation (5) and using centered differences at the grounding line. Besides the momentum velocity calculation within the grounded part, the FGSTS model is identical to the FGSHSF model, thus centered differences are used for the thickness evolution equation at the grounding line. In contrast, for the MGSTS model asymmetric differences are used for the thickness evolution equation at the grounding line, allowing a discontinuity in surface slope. The details for the MGSTS model are given in section 2.2.2.2 and in Appendices A and B.

[61] A basal resistance coefficient of  $\beta^2 = 1.0 \times 10^9 \text{ Pa s m}^{-1}$  is used and the initial lengths of the ice stream and the shelf are set to 750 km and 250 km

respectively. Again, the rate factor used corresponds to  $-10^\circ\text{C}$  and the initial accumulation rate is set to  $0.2 \text{ m a}^{-1}$ .

### 5.1. Steady State Calculations

[62] In contrast to the ice sheet, no analytical or numerical initial steady state solution for the ice stream part is available. We calculate for both models an approximate initial steady state by neglecting the longitudinal stress terms in the ice stream equation (6). Using this solution the models are run forward in time until a steady state is reached (typically after 5 ka). For the FGSTS model, the steady state grounding line position is usually identical to its initial location at 750 km, whereas for the MGSTS model the grounding line has advanced slightly. Note that the elevation at the ice divide is now lower (1400 m) than in the ice sheet case (4500 m) as expected for an ice stream (Figure 9). For some parameter settings, such as smaller dimensions or a smaller  $\beta^2$ , no initial steady state could be found for the MGSTS model.

### 5.2. Perturbation Experiments

[63] The perturbation experiments used with the ice sheet are now repeated with the ice stream/shelf models (FGSTS and MGSTS). In most aspects the results for both models are qualitatively similar to the ice sheet/shelf case.

#### 5.2.1. FGSTS Model

[64] In contrast to the ice sheet case, the FGSTS model has a strong tendency to advance (Figure 16) and no retreat of the grounding line was obtained for a reduction of the accumulation rate to  $0.1 \text{ m a}^{-1}$  or an increase in sea level to +125 m. Only a massive reduction of accumulation to  $0.01 \text{ m a}^{-1}$  leads to a retreat, although it does not start until 25 ka after the step change. However, in all other aspects, the results are qualitatively similar to the ones from the FGSHSF model. A dependency of the grounding line migration on the sign of the basal slope is observed and for a flat or up sloping bed we get an unstable advance (Figure 16). In addition, the grounding line change strongly depends on the horizontal grid size and after switching back the external forcing to the initial value the grounding line does not go back to its initial value. Including lateral drag as before in the FGSHSF model ( $\gamma = 2 \times 10^4 \text{ Pa s m}^{-2}$ ) produces similar qualitative behavior of the grounding line, however if a change does occur it is both faster and larger (Figure 16). The comments above also apply to the results of the sea level change experiments ( $\pm 125 \text{ m}$  over 10 ka).

#### 5.2.2. MGSTS Model

[65] The response of the MGSTS model, shown in Figure 17 for the accumulation change experiment only, is qualitatively similar to the MGSHXX model, although the magnitude of grounding line change (for the same external forcing) is about a factor of five larger than for the MGSHXX model. This higher sensitivity of ice streams to changes in the external forcing is expected to be a result of a lower surface slope behind the grounding line. The MGSTS model is also insensitive to basal slope (Table 4); the grid size dependency is weak and within the accuracy of the model; the experiments are in general reversible; and importantly, the MGSTS model shows a stable behavior. Thus the coupled stream shelf model (MGSTS) shows qualitatively the same dynamics as the MGSHXX model. The analogous dynamics of the

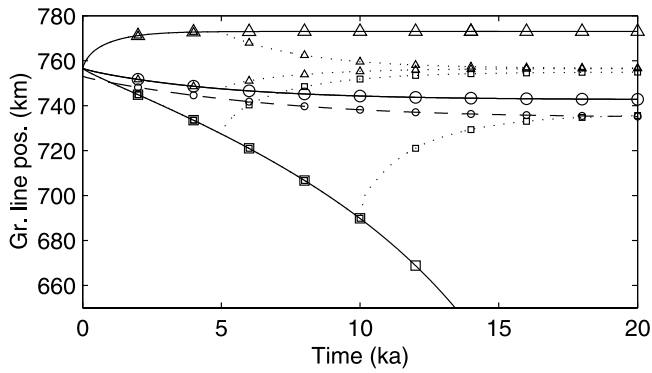


**Figure 17.** Response of the grounding line calculated with the MGSTSF model to a change in accumulation to  $0.1 \text{ m a}^{-1}$  (circles), to  $1.0 \text{ m a}^{-1}$  (triangles), and to  $0.01 \text{ m a}^{-1}$  (squares). The dotted lines refer to the same forcing, but here the accumulation rate is set back to the initial value at 5 ka or 10 ka, respectively. The dashed line refers to a smaller initial grid size of 6.25 km instead of 12.5 km for a change in accumulation to  $0.1 \text{ m a}^{-1}$ .

MGSTSF model does not necessarily mean that mechanical coupling at the grounding line can be ignored. However, it seems that the discretization and grounding line treatment (moving grid) of the MGSTSF model, which are essentially the same as in the MGSXXX model, dominantly determine the dynamics of the grounding line and therefore preserve the stable dynamical behavior from the MGSXXX model and possibly the condition of stable neutral equilibrium. Whether a marine ice sheet which is mechanically coupled to its ice shelf should “theoretically” have neutral equilibrium is not known.

### 5.2.2.1. Unstable Retreat

[66] The one case, in which the results of the MGSTSF model are distinctly different from the MGSXXX model, is for a “strong” retreat. A decrease of the accumulation rate to  $0.01 \text{ m a}^{-1}$  (or lower) results in an unstable retreat of the grounding line for the MGSTSF model and the ice stream vanishes (Figure 17). An unstable retreat is also obtained when the value of the friction coefficient  $\beta^2$  is reduced below  $1.0 \times 10^9 \text{ Pa s m}^{-1}$ . For these “strong” retreats, after switching back  $a$  or  $\beta^2$  at 5 ka or 10 ka to the initial value, the grounding line approaches a steady state, however, this steady state position is not the same as the initial grounding line position (Figure 17). This indicates that these “extreme” experiments are irreversible. No instability was obtained for any advance or any sea level rise or lowering experiment. The experiment for a decrease of the accumulation rate to  $0.01 \text{ m a}^{-1}$  was repeated for the two ice sheet models (MGSXXX and MGSHSF) using a much higher rate factor of  $A = 1.0 \times 10^{-14} \text{ Pa}^{-3} \text{ a}^{-1}$  to simulate an ice sheet with approximately the same initial geometry as the ice stream from the MGSTSF model. No unstable retreat was obtained for this setup, implying that it is not just the ice sheet shape or the lower surface slope that leads to the observed instability. The same experiment has also been repeated with the MGSTSF model but neglecting the longitudinal stress gradients within the grounded part of the stream, meaning that the driving stress is balanced by  $\beta^2 u$  alone (equation (6)). Again, no unstable retreat was

obtained. A further experiment with a modified MGSTSF model that considers longitudinal stress gradients up to one grid point behind the grounding line, and therefore only allows mechanical coupling between shelf and sheet around the grounding line, leads to similar unstable behavior as observed for the full MGSTSF model. The additional model experiments therefore indicate that the retreat instability is not solely a result of the discretization scheme, and grounding line treatment (moving grid) alone, but may be associated with the longitudinal coupling. In case of very low friction coefficients, longitudinal coupling is more effective and one could argue that the ice stream almost becomes an ice shelf [Pattyn, 2003] and the “real” grounding line would then be located at the contact between ice sheet and stream. In our case the stream extends up to the divide and we do not include a sheet which could act as an anchor. Therefore the observed instability for low basal frictions may be due to the fact that the stream becomes an ice shelf (extremely low aspect ratio of the stream).

### 5.2.2.2. Sensitivity to Lateral Drag

[67] Including lateral drag in the floating and grounded part of the MGSTSF model as before in the fixed grid models ( $\gamma = 2 \times 10^4 \text{ Pa s m}^{-2}$  (equation (12))) does not change the qualitative response of the grounding line to the applied external forcing. Furthermore, the amount of grounding line change is almost identical to the case without consideration of lateral drag. This result contrasts the observed significant influence of lateral drag in the fixed grid model (Figure 16).

### 5.2.2.3. Sensitivity to Discretization

[68] Because no shelf is considered in the MGSXXX model the horizontal gradients in the grounding line migration equation (10) are discretized by upstream differences. Upstream differences are also used in the MGSTSF model, however, considering a shelf, we now have the possibility of using central differences to discretize these gradients. Therefore additional MGSTSF model runs have been performed in which centered differences are used for the flux divergence and thickness gradient in equation (10) instead of upstream differences. The steady state geometry from the upstream case is used as an initial condition. In the

**Table 4.** Change in Grounding Line ( $\Delta L_g$ ) Calculated by the MGSTSF Model for Different Basal Slopes<sup>a</sup>

$a_+$ , $\text{m a}^{-1}$	$l_+$ , m	Slope	$\Delta L_g$	
			km	%
<i>Accumulation Step Change</i>				
0.1		up	-13.80	-1.82
0.1		flat	-13.77	-1.82
0.1		down	-13.75	-1.82
1.0		up	16.22	2.14
1.0		flat	16.38	2.17
1.0		down	16.57	2.19
<i>Sea Level Change</i>				
	+125	up	-8.99	-1.18
	+125	flat	-8.98	-1.18
	+125	down	-8.98	-1.19
	-125	up	6.97	0.92
	-125	flat	6.94	0.92
	-125	down	6.91	0.91

<sup>a</sup>The performed experiments are accumulation step changes to  $a_+$  and sea level changes to  $l_+$ .

calculation of a new steady state, the grounding line starts to advance first slowly but then accelerates and does not reach a steady state configuration. For an accumulation step change experiment, we also obtain an unstable retreat or advance using centered differences in equation (10). A close examination shows that it is the centered discretization (instead of upstream) of the flux gradient ( $\partial q/\partial x$ ) in equation (10) that leads to the observed instability not the centered discretization of the thickness gradient ( $\partial h/\partial x$ ). The same sensitivity of the grounding line change to a centered discretization (instead of upstream) of equation (10) is found for the MGSHSF model suggesting that the instability is independent of the mechanical coupling at the grounding line. This sensitivity analysis indicates that the way we discretize the grounding line migration equation in a moving grid model strongly affects the dynamics of the marine ice sheet. One therefore has to be careful with predictions of such moving grid models.

### 5.3. Summary of Ice Stream Experiments

[69] For both the MGSTSF and the FGSTSF models, the results are qualitatively similar to the two ice sheet models. This implies that the way in which the mechanical coupling between the grounded and the floating ice is incorporated into the models does not affect their qualitative behavior. Even the consideration of lateral drag throughout the domain, which allows shelf buttressing, did not alter these results. However, we should note that this insensitivity to longitudinal coupling is only tested here in cases where lateral resistance is low and there are no dramatic changes in ice shelf buttressing.

[70] There are two main differences compared to the dynamics of the sheet models. First, the FGSTSF model shows an advancing tendency independent of the particular rate factor chosen. Second, the “extreme” retreat scenarios lead for the case of the MGSTSH model to an unstable retreat. The FGSTSF model still shows a strong dependency on grid size and basal topography. The insensitivity of the two models to the mechanical coupling at the grounding line suggests that it is the numerics and the way in which grounding line migration is treated in the models that dominates their qualitative dynamics.

## 6. Concluding Discussion

[71] Several previous modeling studies have concentrated on the migration of the grounding line of a marine ice sheet such as the WAIS. The present study presents an extensive comparison of the different numerical methods used to simulate grounding line migration and investigates the sensitivity of their predictions to model numerics. We have selected models that reflect the basic classes of model that have been applied to this problem. The range of models that we have tested can be classified into two ways. First, by the physics that they contain. This range includes models that combine sheet (vertical shear dominated) and shelf (plug) flow, stream (plug) and shelf flow, and sheet flow alone. Second, by the way in which the underlying differential equations are discretized. We are primarily concerned with the differences between fixed and moving grids, although we have also investigated the effects of discretization details near the grounding line. We believe that the fixed grid

models are representative of the models typically used to simulate the past and future behavior of the Antarctic ice sheet [e.g., Ritz *et al.*, 2001; Huybrechts, 2002; Huybrechts and De Wolde, 1999]. We have also investigated the effect of numerical details (such as grid size and time step) on model behavior. We use this as a test of the robustness of a numerical model and expect that a robust model will exhibit behavior that is independent of numerical detail. The predictions of models that show excessive dependence on numerics should therefore be treated with some suspicion.

[72] This study clearly shows that from these models no consensus is reached in how the grounding line should react to changes in boundary conditions such as changes in sea level or the accumulation rate.

[73] In the case of the moving grid models, the changes in grounding line are in general small, a new steady state is always reached (stable system) and the perturbation experiments are reversible. An important result is that the grounding line dynamics are insensitive to basal slope, which therefore questions earlier suggestions of the inherent instability of a marine ice sheet on an up sloping bed [Weertman, 1974; Thomas and Bentley, 1978]. Although the moving grid model is numerically self consistent (shows the condition of neutral equilibrium), grounding line motion is rather sensitive to details of the discretization around the grounding line and it is not clear whether the way the model is setup implicitly biases (controls) the grounding line dynamics. Nonetheless, it can be concluded that this type of model appears to be robust according to our criterion.

[74] The results of the fixed grid model are consistent with the earlier EISMINT results using similar fixed grid models [Huybrechts, 1997] but are in clear contrast to the results of the moving grid models. The fixed grid models show larger changes in grounding line position (in the cases where a change occurs) and the changes are irreversible. Depending on the chosen temperature within the ice, a preference for advance or retreat is observed, which implies that an accurate computation of temperature within the shelf and in the grounding line region is needed for accurate modeling of grounding line migration. Furthermore, the grounding line motion is unstable on a flat or up sloping bed, meaning that the stability of a marine ice sheet strongly depends on the basal slope and/or changes in the cross sectional area. This finding contrasts the stable behavior of the moving grid model and is, of course, important for the dynamics of marine ice sheets such as the WAIS, and supports several early theories predicting instability [Weertman, 1974].

[75] The crucial finding of this study is the strong dependency of the fixed grid model on its numerical details such as the horizontal grid size around the grounding line. This type of model is certainly not robust by our definition. This implies that we should be very careful when interpreting the grounding line predictions from the existing fixed grid marine models, which have been used for several reconstructions of the past evolution of Antarctica [Ritz *et al.*, 2001; Huybrechts, 2002; Huybrechts and De Wolde, 1999; Huybrechts, 1990].

[76] For both methods of treating grounding line migration, the incorporation of mechanical coupling over the grounding line does not change the qualitative behavior of grounding line motion. This finding also holds when lateral

drag is incorporated in the shelf (shelf buttressing). The dynamics of the grounding line are dominantly controlled by the way the grounding line motion is treated and the discretization scheme used, and the physics incorporated into a particular model appears to have only secondary importance (in particular, the longitudinal momentum coupling between the ice shelf and the grounded ice sheet). Thus it is difficult to assess the importance of longitudinal coupling until a reliable numerical method of treating grounding line motion has been established.

[77] The somewhat peculiar grounding line dynamics and the strong grid size dependency observed for the fixed grid model (as opposed to the moving grid model) seems mainly to be a result of having a fixed grid. We therefore doubt whether a fixed grid grounding line motion model can ever be satisfactory. This would favor the use of a moving grid coordinate system that allows the grounding line to be tracked continuously. However, implementing such a stretched grid in a three-dimensional ice sheet model is a very major task. A useful compromise for further development may therefore be a locally adaptive grid. Such a grid would maintain the basic structure of the fixed grid over the large domain of the ice sheet but track the position of the grounding line by local deformation of the overall grid. Although the work here was performed using finite difference models, we expect the same issue of fixed versus moving grid would affect finite element models, although they are better suited to resolve irregular geometries.

[78] We finally conclude that this model comparison study can not conclusively identify a reliable method of treating grounding line migration within numerical ice sheet models. It also demonstrates an urgent need of further development in order to be able to make accurate predictions for the evolution of the WAIS. In particular, the modeling community should find a method of employing a moving grid in two-dimensional plane ice flow models. The experiments performed here could represent a basis for ‘model intercomparison benchmarks’ for models with a moving grounding line. Further model development also requires a better observational history of grounding line migration (in terms of both the timing and spatial extent) and also indicates the need of a test data set for the modeling community.

## Appendix A: Coordinate Transformations

### A1. MGSXX Model

[79] Owing to the coordinate transformation  $(x, t) \rightarrow (\xi, \tau)$  given by  $\xi \equiv x/L_g$  and  $\tau \equiv t$  the function derivatives transform to

$$\frac{\partial}{\partial x} = \frac{\partial \xi}{\partial x} \frac{\partial}{\partial \xi} = \frac{1}{L_g} \frac{\partial}{\partial \xi} \quad (\text{A1})$$

$$\frac{\partial}{\partial t} = \frac{\partial}{\partial \tau} + \frac{\partial \xi}{\partial t} \frac{\partial}{\partial \xi} = \frac{\partial}{\partial \tau} - \frac{\dot{L}_g}{L_g} \xi \frac{\partial}{\partial \xi}. \quad (\text{A2})$$

The surface evolution equation (1) then gets

$$\frac{\partial h}{\partial \tau} = a - \frac{1}{L_g} \frac{\partial q}{\partial \xi} + \frac{\dot{L}_g}{L_g} \xi \frac{\partial h}{\partial \xi}, \quad (\text{A3})$$

and equation (10) for the grounding line migration rate gets

$$\dot{L}_g = \frac{L_g \frac{\rho_w}{\rho_i} \frac{\partial f}{\partial \tau} + \frac{\partial q}{\partial \xi} - L_g a}{\frac{\partial h}{\partial \xi} - \frac{\rho_w}{\rho_i} \frac{\partial f}{\partial \xi}}, \quad (\text{A4})$$

where all quantities are evaluated at the grounding line position. The vertically averaged velocity  $u$  in the ice sheet (equation (2)) is in the  $\xi$  coordinate system given by

$$u = C \left( \frac{1}{L_g} \right)^n \left( \frac{\partial s}{\partial \xi} \right)^n h^{n+1}. \quad (\text{A5})$$

### A2. MGSTSF Model

[80] Owing to the stepwise coordinate transformation  $(x, t) \rightarrow (\xi, \tau)$  given by equation (11) and  $\tau \equiv t$  the function derivatives transform for the case of a fixed ice shelf position ( $dL_{\text{tot}}/dt = 0$ ,  $dL_g/dt = dL_s/dt$ ) to

$$\frac{\partial}{\partial x} = \frac{\partial \xi}{\partial x} \frac{\partial}{\partial \xi} = \frac{r}{L_g} \frac{\partial}{\partial \xi} \quad (\text{A6})$$

$$\frac{\partial}{\partial t} = \frac{\partial}{\partial \tau} + \frac{\partial \xi}{\partial t} \frac{\partial}{\partial \xi} = \frac{\partial}{\partial \tau} - \frac{\dot{L}_g}{L_g} \xi \frac{\partial}{\partial \xi} \quad (\text{A7})$$

for the grounded part and to

$$\frac{\partial}{\partial x} = \frac{\partial \xi}{\partial x} \frac{\partial}{\partial \xi} = \frac{1-r}{L_s} \frac{\partial}{\partial \xi} \quad (\text{A8})$$

$$\frac{\partial}{\partial t} = \frac{\partial}{\partial \tau} + \frac{\partial \xi}{\partial t} \frac{\partial}{\partial \xi} = \frac{\partial}{\partial \tau} - \frac{(\xi-1)\dot{L}_g}{L_s} \frac{\partial}{\partial \xi} \quad (\text{A9})$$

for the floating part. The thickness evolution equation (1) in the  $\xi$  coordinate system is for the grounded part

$$\frac{\partial h}{\partial \tau} = a - \frac{r}{L_g} \frac{\partial q}{\partial \xi} - \frac{\dot{L}_g}{L_g} \frac{\partial h}{\partial \xi} \quad (\text{A10})$$

and for the floating part

$$\frac{\partial h}{\partial \tau} = a - \frac{1-r}{L_s} \frac{\partial q}{\partial \xi} - \frac{(\xi-1)\dot{L}_g}{L_s} \frac{\partial h}{\partial \xi}. \quad (\text{A11})$$

The equation for the grounding line migration rate (10) is then

$$\dot{L}_g = \frac{\frac{L_g}{r} \frac{\rho_w}{\rho_i} \frac{\partial f}{\partial \tau} + \frac{\partial q}{\partial \xi} - \frac{L_g}{r} a}{\frac{\partial h}{\partial \xi} - \frac{\rho_w}{\rho_i} \frac{\partial f}{\partial \xi}}. \quad (\text{A12})$$

The ice shelf equation (4) in the  $\xi$  coordinate system is given by

$$\frac{(1-r)}{L_s} 2 \frac{\partial}{\partial \xi} h v \frac{\partial u}{\partial \xi} = \rho_i g h \frac{\partial s}{\partial \xi}, \quad (\text{A13})$$

with

$$v = A^{-1/n} \left[ \left( \frac{(1-r)}{L_s} \frac{\partial u}{\partial x} \right)^2 \right]^{(1-n)/(2n)}, \quad (\text{A14})$$

and the transformed ice stream equation (6) is

$$\frac{r}{L_g} 2 \frac{\partial}{\partial \xi} h v \frac{\partial u}{\partial \xi} - \frac{L_g}{r} \beta^2 u = \rho_i g h \frac{\partial s}{\partial \xi}, \quad (\text{A15})$$

with the effective viscosity

$$v = A^{-1/n} \left[ \left( \frac{r}{L_g} \frac{\partial u}{\partial x} \right)^2 \right]^{(1-n)/(2n)}. \quad (\text{A16})$$

Note that in the case  $r = 1$ , the equations above correspond to an ice stream without a shelf.

## Appendix B: Discretization

### B1. Fixed Grid Models

[81] The fluxes and the velocities in the thickness evolution equation (1) are calculated on a staggered grid and are given by

$$q_{i+1/2} = u_{i+1/2} \frac{h_{i+1} + h_i}{2} \quad (\text{B1})$$

$$u_{i+1/2} = C \left( \frac{s_{i+1} - s_i}{\Delta x} \right)^n h^{n+1}, \quad (\text{B2})$$

where  $i$  is the position index with  $i \pm 1/2$  denoting the position on the staggered grid.

### B2. Moving Grid Models

#### B2.1. MGSHXX Model

[82] Following the discretization scheme suggested by *LeMeur and Hindmarsh* [2001] and *Hindmarsh and LeMeur* [2001] the fluxes are calculated on a staggered grid and the grounding line migration equation (A4) is given by

$$\dot{L}_g^k = \frac{L_g^k \frac{\rho_w}{\rho_i} \left( \frac{f_m^k - f_{m-1}^{k-1}}{\Delta t} \right) + (q_{m-1/2}^k - q_{m-3/2}^k) - L_g^k a}{D_5 + \frac{\rho_w}{\rho_i} \frac{f_{m+1}^k - f_{m-1}^k}{2\Delta \xi}}, \quad (\text{B3})$$

where  $\Delta \xi$  is the grid size in the stretched coordinate system,  $m$  is the position index of the grounding line with  $m \pm 1/2$  denoting the position on the staggered grid and  $k$  is the time index.  $D_5$  is the fifth-order backward-

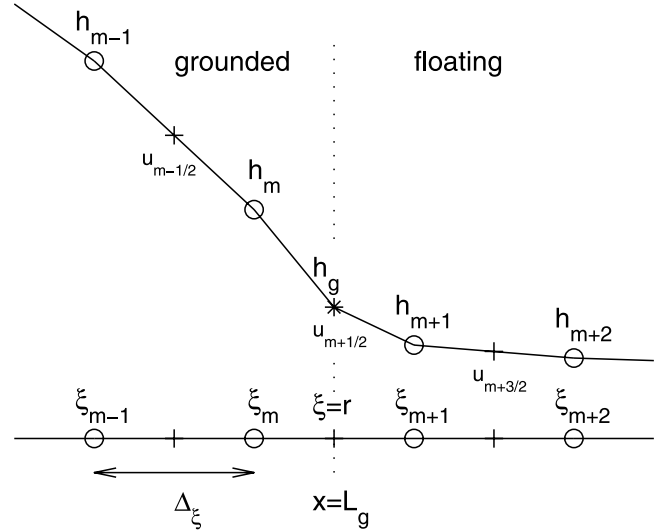


**Figure B1.** Schematic of the discretization around the grounding line for the MGSTSF model and the MGSHSF model. Note that the grounding line (star,  $x = L_g$ ) is on the staggered grid on which the velocities and fluxes are calculated.

difference approximation of the thickness slope at the grounding line given by

$$D_5 = \frac{1}{60\Delta \xi} \left( 137h_n^k - 300h_{n-1}^k + 300h_{n-2}^k - 200h_{n-3}^k + 75h_{n-4}^k - 12h_{n-5}^k \right). \quad (\text{B4})$$

The thickness evolution equation (A3) gets

$$h_i^{k+1} = h_i^k + \Delta t \left( a_i^k - \frac{q_{i+1/2}^k - q_{i-1/2}^k}{L_g^k} + \xi_i \frac{\dot{L}_g^k}{L_g^k \Delta \xi} \frac{(h_{i+1}^k - h_{i-1}^k)}{2\Delta \xi} \right). \quad (\text{B5})$$

The fluxes are given by equation (B1), except at the grounding line ( $i = m + 1/2$ ), where the flux is calculated as

$$q_{m+1/2} = u_{m+1/2} h_g. \quad (\text{B6})$$

The velocities on the staggered grid are given by

$$u_{i+1/2} = C \left( \frac{1}{L_g} \frac{(s_{i+1}^k - s_i^k)}{\Delta \xi} \right)^n \left( \frac{h_{i+1} + h_i}{2} \right)^{n+1}. \quad (\text{B7})$$

#### B2.2. MGSTSF Model

[83] As in the MGSHXX model the flux  $q$  is calculated on a staggered grid in between the grid points where the thickness and surface evolution is calculated. The main difference is now that the position of the grounding line  $L_g$  is located on the staggered grid (Figure B1). The reason for this is to ensure continuity of mass over the grounding line. The additional version of a sheet model with a shelf (noted as MGSHSF) uses the same discretization scheme.

[84] In the  $x$  direction, there are now  $n + 1$  grid points with index  $i \in (0, n)$  and in general the index  $m$  denotes the last grounded regular grid point. The grounding line itself, where flotation is reached is however in between the grid points  $m$  and  $m + 1$  (Figure B1). For the grounding line migration equation (A12) the horizontal gradients for the thickness and the flux are again taken upstream and the discretized grounding line migration equation is given by

$$\dot{L}^k = \frac{L^k \frac{\rho_w f_n^k - f_n^{k-1}}{\Delta t} + (q_{m+1/2}^k - q_{m-1/2}^k) - L_g^k a}{D_{5a} + \frac{\rho_w f_{n+1}^k - f_{n-1}^k}{\rho_i 2\Delta\xi}}, \quad (\text{B8})$$

where  $D_{5a}$  is the fifth-order asymmetric backward-difference approximation of the thickness slope at the grounding line (following *Jacobson* [1999, p. 161]) given by

$$D_{5a} = \frac{1}{60\Delta\xi} (214.476h_g^k - 295.313h_m^k + 131.250h_{m-1}^k - 70.875h_{m-2}^k + 24.107h_{m-3}^k - 3.646h_{m-4}^k). \quad (\text{B9})$$

The thickness evolution equation (A10) is for the grounded part discretized by

$$h_i^{k+1} = h_i^k + \Delta t \left( a_i^k - \frac{r}{L_g^k \Delta\xi} (q_{i+1/2}^k - q_{i-1/2}^k) + \frac{\xi L_g^k (h_{i+1}^k - h_{i-1}^k)}{L_g^k 2\Delta\xi} \right) \quad (\text{B10})$$

and for the shelf part (equation (A11)) by

$$h_i^{k+1} = h_i^k + \Delta t \left( a_i^k - \frac{(1-r)}{L_s^k \Delta\xi} (q_{i+1/2}^k - q_{i-1/2}^k) + \frac{(1-r)L_g^k (h_{i+1}^k - h_{i-1}^k)}{L_s^k 2\Delta\xi} \right). \quad (\text{B11})$$

[85] For the slope of the thickness in equations (A10) and (A11) at the grid points immediately up and down glacier of the grounding line (indices  $m$  and  $m + 1$ ) asymmetric central differences are used given by

$$\left. \frac{\partial h}{\partial x} \right|_m = \frac{4h_g - 3h_m - h_{m-1}}{3\Delta\xi} \quad (\text{B12})$$

and

$$\left. \frac{\partial h}{\partial x} \right|_{m+1} = \frac{h_{m+2} + 3h_{m+1} - 4h_g}{3\Delta\xi}. \quad (\text{B13})$$

As in the MGSXX model the fluxes  $q_{i+1/2}$  are given by equation (B1) at the grounding line, except at the grounding line ( $i = m + 1/2$ ), where the flux is given by equation (B6).

[86] The vertically averaged velocity for the stream shelf system is calculated from the equations (A13) and (A15) by iterating for the effective viscosity  $\nu$ . The

discretized version of equation (A15) for the grounded part (stream) is given by

$$\frac{2r}{\Delta\xi^2 L_g} [h_{i+1} \nu_{i+1} (u_{i+3/2} - u_{i+1/2}) - h_i \nu_i (u_{i+1/2} - u_{i-1/2})] - \frac{L_g}{r} \beta^2 u_{i+1/2} = \rho_i g \frac{h_{i+1} + h_i}{2} \frac{s_{i+1} + s_i}{\Delta\xi} \quad (\text{B14})$$

and of equation (A13) for the floating part (shelf) by

$$\frac{2(1-r)}{\Delta\xi^2 L_g} [h_{i+1} \nu_{i+1} (u_{i+3/2} - u_{i+1/2}) - h_i \nu_i (u_{i+1/2} - u_{i-1/2})] = \rho_i g \frac{h_{i+1} + h_i}{2} \frac{s_{i+1} + s_i}{\Delta\xi}. \quad (\text{B15})$$

At the grounding line itself ( $i = m + 1/2$ ) we use upstream differences for the surface slope (on the right-hand side) and we get

$$\frac{2}{\Delta\xi^2} \left[ \frac{1-r}{L_s} h_{m+1} \nu_{m+1} (u_{m+3/2} - u_{m+1/2}) - \frac{r}{L_g} h_i \nu_m (u_{m+1/2} - u_{m-1/2}) \right] - \frac{L_g}{r} \beta^2 u_{m+1/2} = \rho_i g h_m \frac{s_{m-1/2} + s_m}{\Delta\xi/2}. \quad (\text{B16})$$

## Notation

$x$	and horizontal coordinate in flow direction (m).
$z$	vertical coordinate (m).
$\Delta_x$	and horizontal grid size (m).
$\xi$	normalized horizontal coordinate (dimensionless).
$\Delta_\xi$	normalized horizontal grid size (dimensionless).
$h$	ice thickness (m).
$s$	surface elevation (m).
$b$	elevation of ice sheet base (m).
$f$	water depth at grounding line (m).
$l$	sea level (m).
$L_{\text{tot}}$	distance of shelf front from ice divide (m).
$L_g$	distance of grounding line from ice divide (m).
$L_s$	shelf length (m).
$\dot{L}_g$	grounding line migration rate ( $\text{m a}^{-1}$ ).
$r$	position of grounding line in $\xi$ coordinate system (dimensionless).
$u$	vertically averaged horizontal velocity ( $\text{m a}^{-1}$ ).
$q$	vertically integrated horizontal ice flux ( $\text{m}^2 \text{a}^{-1}$ ).
$t$	time (a).
$\Delta t$	time step (a).
$\tau$	time in $\xi$ coordinate system (a).
$a$	surface accumulation rate ( $\text{m a}^{-1}$ ).
$g$	acceleration due to gravity ( $9.81 \text{ m s}^{-2}$ ).
$\rho_i$	density of ice ( $910 \text{ kg m}^{-3}$ ).
$\rho_w$	density of ocean water ( $1028 \text{ kg m}^{-3}$ ).
$n$	flow law exponent ( $\equiv 3$ ).
$A$	rate factor ( $\text{Pa}^{-3} \text{ s}^{-1}$ ).
$\nu$	vertically averaged effective viscosity (Pa s).
$\dot{\epsilon}$	vertically averaged effective strain rate ( $\text{a}^{-1}$ ).

- $C$  constant given by equation (3).  
 $\beta^2$  basal friction coefficient ( $\text{Pa s m}^{-1}$ ).  
 $\gamma$  lateral friction coefficient.  
 $W$  ice stream/shelf width (m).

[87] **Acknowledgments.** We thank G. Clarke and two anonymous reviewers for the useful comments and are grateful to R. Hindmarsh for helpful discussions. This research was funded by the U.K. Natural Environment Research Council's standard grant NER/A/S/2000/00419 (Pine Island Glacier flow and dynamics) and by the Centre for Polar Observation and Modelling.

## References

- Alley, R. B., and R. A. Bindschadler (2001), The West Antarctic ice sheet and sea-level change, in *The West Antarctic Ice Sheet: Behavior and Environment*, *Antarct. Res. Ser.*, vol. 77, edited by R. B. Alley and R. A. Bindschadler, pp. 1–11, AGU, Washington, D. C.
- Anderson, J. B., and S. S. Shipp (2001), Evolution of the West Antarctic ice sheet, in *The West Antarctic Ice Sheet: Behavior and Environment*, *Antarct. Res. Ser.*, vol. 77, edited by R. B. Alley and R. A. Bindschadler, pp. 45–57, AGU, Washington, D. C.
- Bentley, C. R. (1997), Rapid sea-level rise soon from West Antarctic ice sheet collapse?, *Science*, *275*, 1077–1078.
- Bentley, C. R. (1998), Rapid sea-level rise from a West Antarctic ice-sheet collapse: A short-term perspective, *J. Glaciol.*, *44*, 157–163.
- Conway, H., B. L. Hall, G. H. Denton, A. M. Gades, and E. D. Waddington (1999), Past and future grounding-line retreat of the West Antarctic ice sheet, *Science*, *286*, 280–283.
- Echelmeyer, K. A., W. Harrison, C. Larsen, and J. E. Mitchell (1994), The role of the margins in the dynamics of an active ice stream, *J. Glaciol.*, *40*, 527–538.
- Glen, J. W. (1955), The creep of polycrystalline ice, *Proc. R. Soc. London, Ser. A*, *228*, 519–538.
- Hindmarsh, R. C. A. (1993), Qualitative dynamics of marine ice sheets, in *Ice in the Climate System*, *NATO Sci. Ser.*, vol. 1, edited by W. R. Peltier, pp. 67–99, N. Atlantic Treaty Organ., Brussels.
- Hindmarsh, R. C. A. (1996), Stability of ice rises and uncoupled marine ice sheets, *Ann. Glaciol.*, *23*, 105–115.
- Hindmarsh, R. C. A., and E. LeMeur (2001), Dynamical processes involved in the retreat of marine ice sheets, *J. Glaciol.*, *47*, 271–282.
- Hutter, K. (1983), *Theoretical Glaciology*, Springer, New York.
- Huybrechts, P. (1990), A 3-D model for the Antarctic ice sheet: A sensitivity study on the glacial interglacial contrast, *Clim. Dyn.*, *5*, 79–92.
- Huybrechts, P. (1992), The Antarctic ice sheet and environmental change: A three-dimensional modeling study, *Ber. Polarforsch.*, *99*, 241 pp.
- Huybrechts, P. (1997), Report of the third EISMINT workshop on model intercomparison, report, EISMINT Intercomparison Group, Grindelwald, Switzerland.
- Huybrechts, P. (2002), Sea-level changes at the LGM from ice-dynamic reconstructions of the Greenland and Antarctic ice sheets during the last glacial cycles, *Quat. Sci. Rev.*, *21*, 203–231.
- Huybrechts, P., and J. De Wolde (1999), The dynamic response of the Greenland and Antarctic ice sheet to multiple-century climatic warming, *J. Clim.*, *12*, 2169–2188.
- Jacobson, M. Z. (1999), *Fundamentals of Atmospheric Modeling*, Cambridge Univ. Press, New York.
- LeMeur, E., and R. C. A. Hindmarsh (2001), Coupled marine-ice-sheet/Earth dynamics using a dynamically consistent ice-sheet model and a self-gravitating viscous Earth model, *J. Glaciol.*, *47*, 258–270.
- MacAyeal, D. R., R. A. Bindschadler, and T. A. Scambos (1995), Basal friction of Ice Stream E, West Antarctica, *J. Glaciol.*, *41*, 247–262.
- Paterson, W. S. B. (1994), *The Physics of Glaciers*, 3rd ed., 380 pp., Elsevier, New York.
- Paterson, W. S. B., and W. F. Budd (1982), Flow parameters for ice sheet modelling, *Cold Reg. Sci. Technol.*, *6*, 175–177.
- Pattyn, F. (2003), A new three-dimensional higher-order thermomechanical ice sheet model: Basic sensitivity, ice stream development, and ice flow across subglacial lakes, *J. Geophys. Res.*, *108*(B8), 2382, doi:10.1029/2002JB002329.
- Press, W. H., S. A. Teukolsky, W. Vetterling, and B. Flannery (1992), *Numerical Recipes in Fortran: The Art of Scientific Computing*, 2nd ed., 963 pp., Cambridge Univ. Press, New York.
- Ritz, C., V. Rommelaere, and C. Dumas (2001), Modeling the evolution of Antarctic ice sheet over the last 420,000 years: Implications for altitude changes in the Vostok region, *J. Glaciol.*, *106*, 31,943–31,964.
- Siegert, M. J., and J. A. Dowdeswell (2002), Late Weichselian iceberg, meltwater and sediment production from the Eurasian High Arctic ice sheet: Results from numerical ice-sheet modelling, *Mar. Geol.*, *188*, 109–127.
- Thomas, R. H., and C. R. Bentley (1978), A model for Holocene retreat of the West Antarctic ice sheet, *Quat. Res.*, *10*, 150–170.
- Van der Veen, C. J. (1985), Response of a marine ice sheet to changes at the grounding line, *Quat. Res.*, *24*, 257–267.
- Van der Veen, C. J., and I. M. Whillans (1996), Model experiments on the evolution and stability of ice streams, *Ann. Glaciol.*, *23*, 129–137.
- Weertman, J. (1974), Stability of the junction of an ice sheet and an ice shelf, *J. Glaciol.*, *13*, 3–11.
- Whillans, I. M., and C. J. Van der Veen (1993), New improved determinations of velocity of Ice Streams B and C, West Antarctica, *J. Glaciol.*, *39*, 483–490.
- Whillans, I. M., and C. J. Van der Veen (1997), The role of lateral drag in the dynamics of Ice Stream B, Antarctica, *J. Glaciol.*, *43*, 231–237.

A. J. Payne and A. Vieli, Centre for Polar Observation and Modelling, School of Geographical Sciences, University of Bristol, University Road, Bristol BS8 1SS, UK. (a.j.payne@bristol.ac.uk; a.vieli@bristol.ac.uk)